Supporting Information for

Enhancement of Association Constants of Various Charge-Transfer Complexes in Siloxane Solvents

Shogo Amemori, *,[a,b,c] Ryosuke Hamamoto, [d] and Motohiro Mizuno*, [a,b,c]

[a]Nanomaterials Research Institute(NanoMaRI), Kanazawa University, Kanazawa 920-1192, Japan

[b]Graduate School of Natural Science and Technology, Kanazawa University, Kanazawa 920-1192, Japan

[c]Institute for Frontier Science Initiative, Kanazawa University, Kanazawa 920-1192, Japan

[d]School of Chemistry, College of Science and Engineering, Kanazawa University, Kanazawa 920-1192, Japan

E-mail: amemori@stuff.kanazawa-u.ac.jp; mizuno@se.kanazawa-u.ac.jp.

Instrumentation

 ^{1}H and ^{13}C NMR measurements were recorded on a Bruker Avance Neo 400 instrument (^{1}H 400 MHz and ^{13}C 100 MHz). UV/Vis spectra were recorded on a JASCO V-750 spectrometer with a JASCO ETCS-761 temperature controller. Elemental analysis and FAB mass spectroscopy were performed at the Research Institute for Instrumental Analysis, Advanced Science Research Center, Kanazawa University.

Materials.

All reagents and solvents for synthesis and measurement were used as received without further purification. 2,6-Dichloro-1,4-benzoquinone (**DCBQ**) (>97%(NMR)) and *n*-hexane (Spectrochemical Analysis grade, >97%(Capillary GC)) was purchased from FUJIFILM Wako Pure Chemical Corporation. 1,2-Diethoxybenzene (**DEB**) (>98%(GC)), 2-isobutoxynaphthalene (**Nap**) (>98%(GC)) and octamethyltrisiloxane (OMTS) (>98%(GC)) were purchased from Tokyo Chemical Industry Co ., Ltd. Poly(dimethylsiloxane) (PDMS) (M_n = 2000 g/mol) was purchased from Sigma-Aldrich. **PMDISi** and **PySi** were synthesized by previously reported methods.[1]
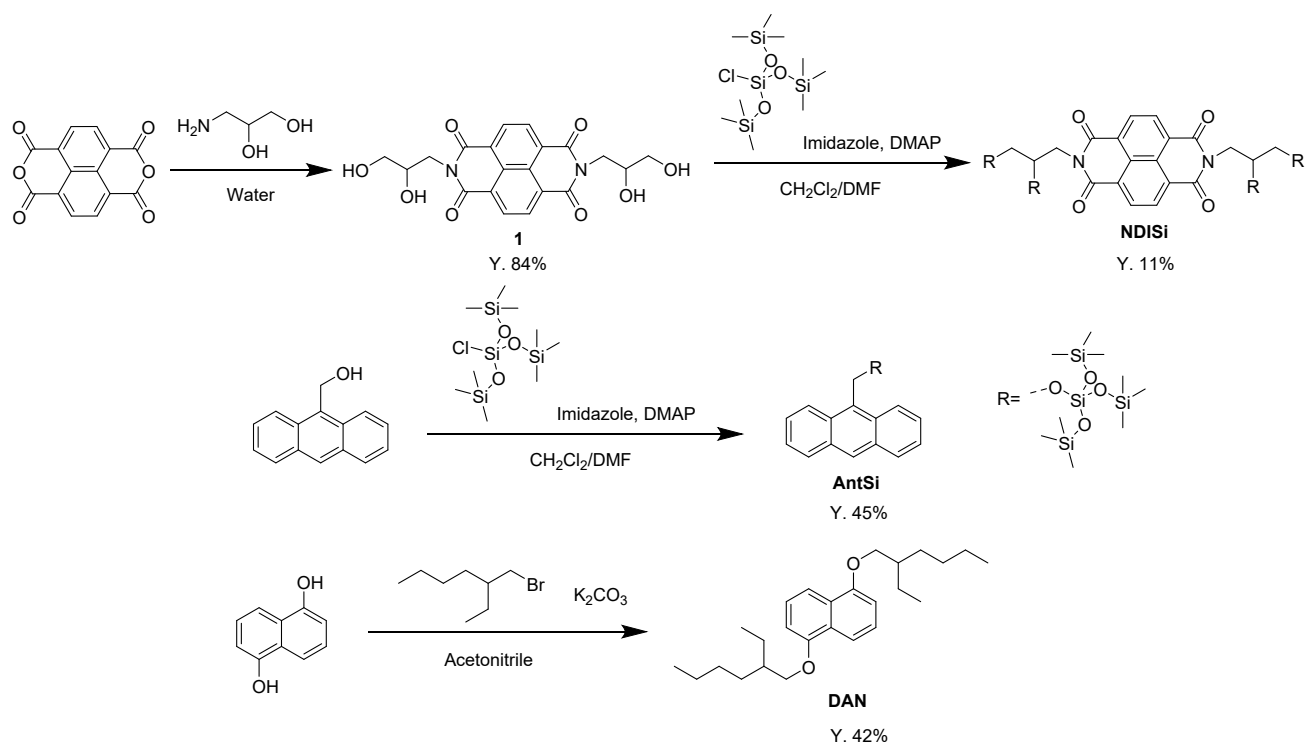
Scheme S1. Synthetic schemes of **NDISi**, **AntSi** and **DAN**.

Synthesis of **1**
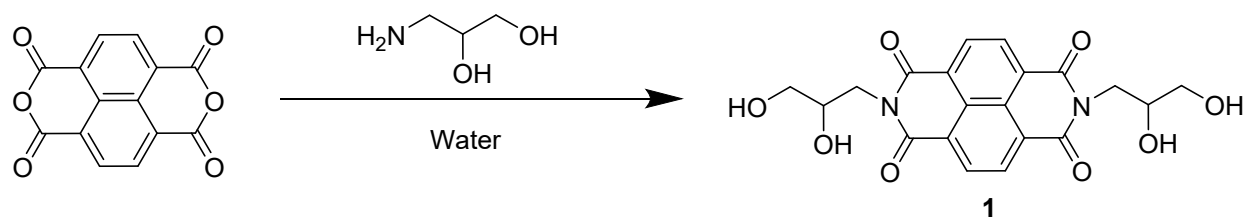
Naphthalenetetracarboxylic dianhydride (2.68 g, 10 mmol) and 3-amino-1,2-propanediol (3.64 g, 40 mmol) in water (30 mL) was heated at 80 °C for 1day. After the reaction mixture was cooled to room temperature, it was filtrated and washed with water. The residue was dried in vacuo to obtain compound **1** as white solid (3.47 g, 8.4 mmol, 84%). ^{1}H NMR (400 MHz, DMSO-d_6, TMS standard): δ (ppm) 3.39-3.49 (m, 4 H, CH_2), 3.89-3.98 (m, 2 H, CH), 4.02 (dd, J = 4.7, 12.9 Hz, 2 H, CH_2), 4.25 (dd, J = 8.5, 12.9 Hz, 2 H, CH_2), 4.63 (br-s, 2 H, OH), 4.84 (br-s, 2 H, OH), 8.66 (s, 4 H, ArH). ^{13}C NMR (100 MHz, DMSO-d_6, TMS standard): δ (ppm) 43.67, 64.40, 68.21, 126.03, 126.27, 130.26, 162.81. HRMS(FAB) Calcd for $C_{20}H_{19}N_2O_8$ [(M+H)$^+$]: m/z 415.1141, Found: m/z 415.1139.
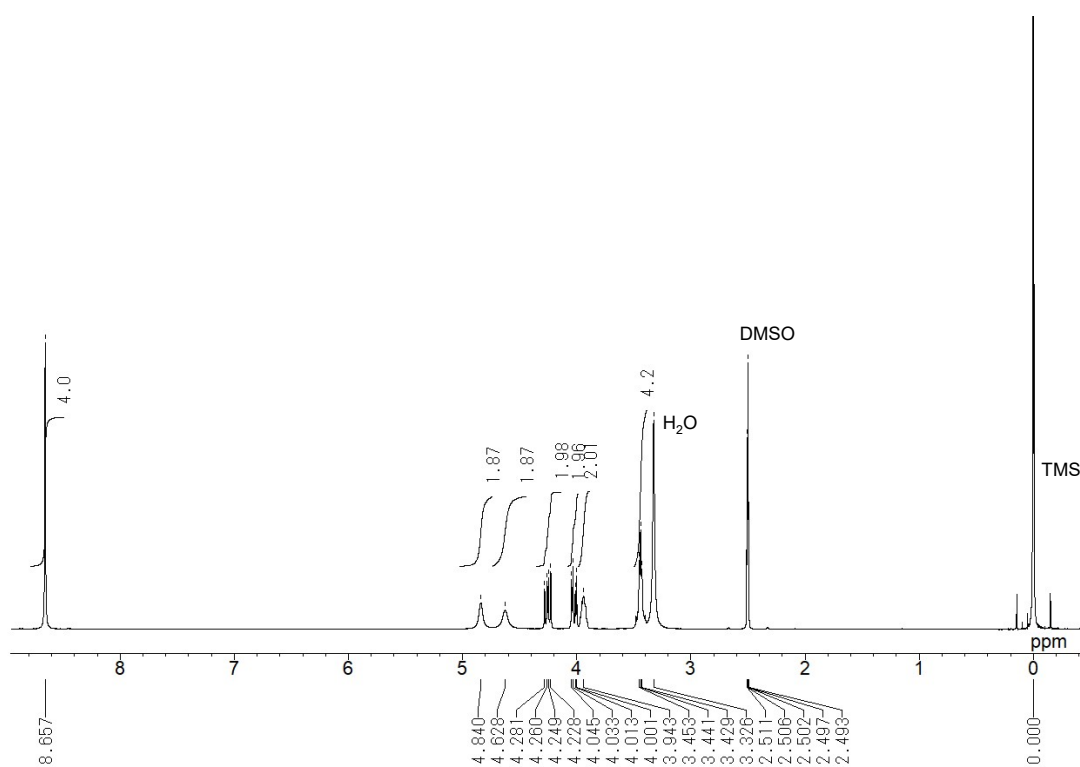
^{1}H NMR spectrum (400 MHz, DMSO-d_6, TMS standard) of **1**.

^{13}C NMR spectrum (100 MHz, DMSO-d_6, TMS standard) of **1**.

Synthesis of **NDISi**

To a solution of **1** (1.24 g, 3.0 mmol), 4-dimethylaminopyridine (37 mg, 0.3 mmol) and imidazole (1.63 g, 24.0 mmol) in dry DMF (4.5 mL) and dry CH$_2$Cl$_2$ (12 mL), tris(trimethylsiloxy)chlorosilane (4.95 mL, 13.8 mmol) was slowly added at 0 °C under N$_2$. After the mixture was stirred for 11 h at room temperature, it was poured into water and extracted with hexane/EtOAc (2/1). The organic layer was washed with water and dried over anhydrous Na$_2$SO$_4$, followed by evaporation to dryness. The residue was purified by column chromatography (SiO$_2$, hexane/dichloromethane=3/1 to 2/1) to obtain **NDISi** as a white solid (0.51 g, 0.32 mmol, 11 %).

^{1}H NMR (400 MHz, CDCl$_3$, TMS standard): δ (ppm) -0.09 (s, 54 H, CH_3), 0.13 (s, 54 H, CH_3), 3.66 (dd, J = 8.2, 9.9 Hz, 2 H, CH_2), 3.91 (dd, J = 4.5, 9.9 Hz, 2 H, CH_2), 4.28 (dd, J = 3.5, 12.9 Hz, 2 H, CH_2), 4.42-4.49 (m, 2 H, CH), 4.57 (dd, J = 9.3, 12.9 Hz, 2 H, CH_2), 8.74 (s, 4 H, ArH). ^{13}C NMR (100 MHz, CDCl$_3$, TMS standard): δ (ppm) 1.39, 1.59, 44.30, 65.47, 69.34, 126.70, 126.83, 130.84, 162.84. HRMS(FAB) Calcd for C$_{56}$H$_{123}$N$_2$O$_{20}$Si$_{16}$ [(M+H)$^+$]: m/z 1591.4977, Found: m/z 1591.4941. Elemental analysis; calculated for C$_{56}$H$_{122}$N$_2$O$_{20}$Si$_{16}$: C 42.22, H 7.72, N 1.76, Found: C 41.90, H 7.33, N 1.81.

^{1}H NMR spectrum (400 MHz, CDCl$_3$, TMS standard) of **NDISi**.

^{13}C NMR spectrum (100 MHz, CDCl$_3$, TMS standard) of **NDISi**.

Synthesis of **AntSi**
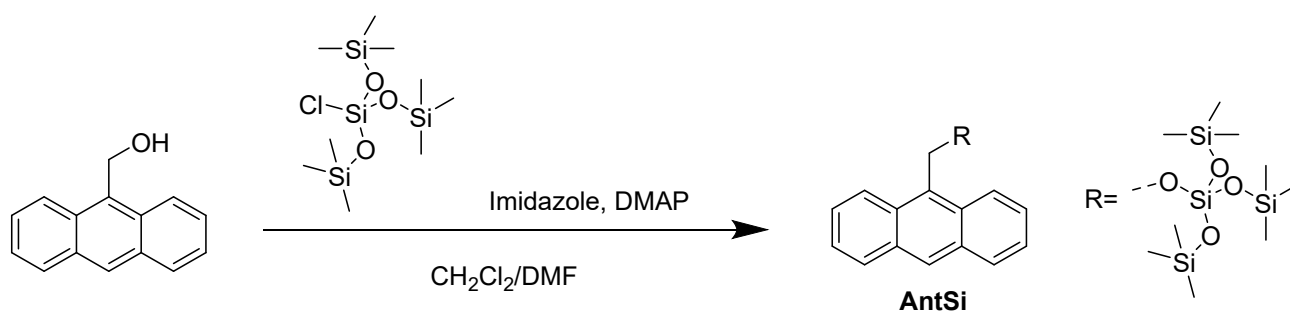
To a solution of 9-anthracenemethanol (1.67 g, 8.0 mmol), 4-dimethylaminopyridine (18 mg, 0.15 mmol) and imidazole (1.09 g, 16.0 mmol) in dry DMF (13 mL) and dry CH_2Cl_2 (32 mL), tris(trimethylsiloxy)chlorosilane (3.3 mL, 9.2 mmol) was slowly added at 0 °C under N_2. After the mixture was stirred for 5 h at room temperature, it was poured into water and extracted with hexane/EtOAc (4/1). The organic layer was dried over anhydrous $MgSO_4$ and evaporated to give a yellow oil. The obtained oil was chromatographed (SiO_2, hexane/EtOAc=99/1 to 98/2) to obtain **AntSi** as a yellow solid (1.81 g, 3.6 mmol, 45%).

^{1}H NMR (400 MHz, $CDCl_3$, TMS standard): δ (ppm) 0.06 (s, 27 H, CH_3), 5.70 (s, 2 H, CH_2), 7.43-7.48 (m, 2 H, ArH), 7.49-7.54 (m, 2 H, ArH), 8.00 (dd, J = 1.3, 8.4 Hz, 2 H, ArH), 8.42-8.46 (m, 3 H, ArH). ^{13}C NMR (100 MHz, $CDCl_3$, TMS standard): δ (ppm) 1.49, 57.57, 124.84, 124.86, 125.71, 127.80, 128.83, 130.59, 131.07, 131.57. HRMS(FAB) Calcd for $C_{24}H_{38}O_4Si_4$ [M$^+$]: m/z 502.1847, Found: m/z 502.1848. Elemental analysis; calculated for $C_{24}H_{38}O_4Si_4$: C 57.32, H 7.62, Found: C 57.11, H 7.50.
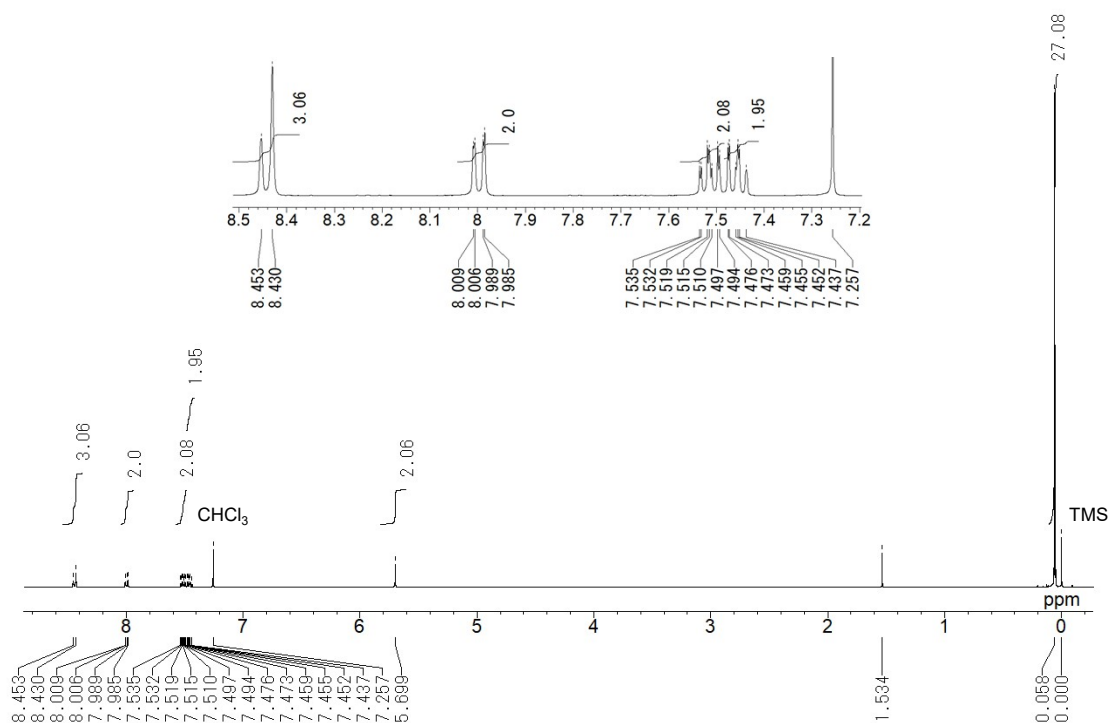
^{1}H NMR spectrum (400 MHz, $CDCl_3$, TMS standard) of **AntSi**.
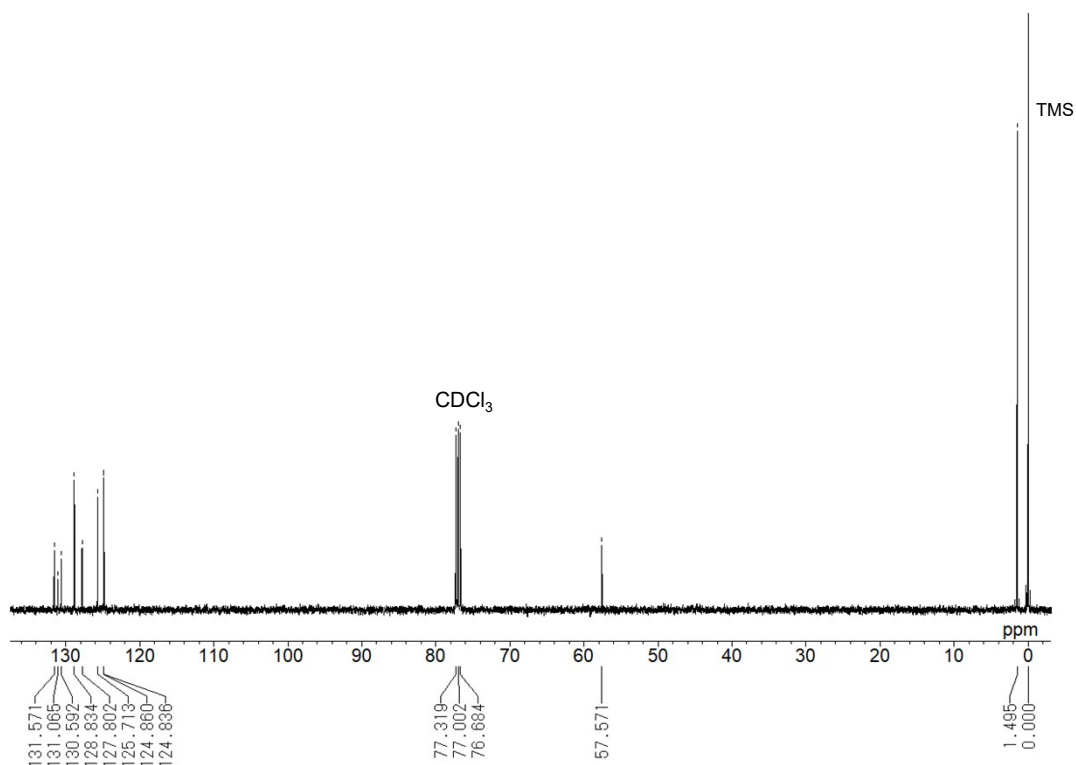
^{13}C NMR spectrum (100 MHz, CDCl$_3$, TMS standard) of **AntSi**.

Synthesis of **DAN**[2]

DAN
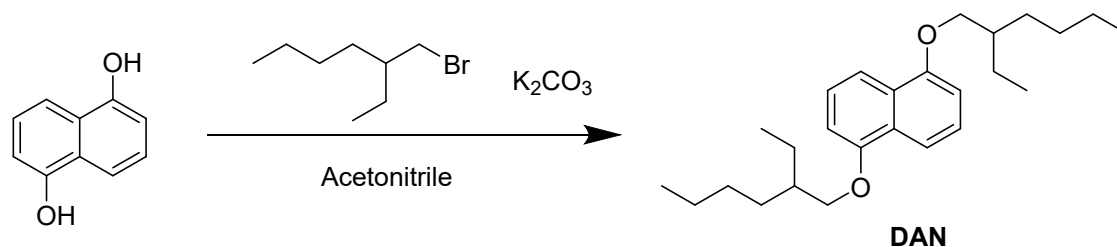
Under N$_2$, the mixture of 1,5-dihydroxynaphthalene (1.60 g, 10.0 mmol), 2-ethylhexyl bromide (7.72 g, 40.0 mmol), potassium carbonate (11.05 g, 80.0 mmol) and dry acetonitrile (80 mL) was refluxed for 24h. After cooling to the room temperature, the resulting mixture was poured into water and extracted with hexane. The organic layer was washed with water and dried over anhydrous MgSO$_4$ followed by evaporation to dryness. The obtained oil was purified by silica gel column chromatography (hexane) and size exclusion chromatography to obtain **DAN** as a colorless solid (1.62 g, 4.2 mmol, 42%).

^{1}H NMR (400 MHz, CDCl$_3$, TMS standard): δ (ppm) 0.91 (t, J =7.1 Hz, 6 H, CH_3), 0.97 (t, J =7.5 Hz, 6 H, CH_3), 1.29-1.42 (m, 8 H, CH_2), 1.44-1.68 (m, 8 H, CH_2), 1.86 (sep, J =6.1 Hz, 2 H, CH), 4.02 (dd, J =1.7, 5.5 Hz, 4 H, CH_2), 6.83 (d, J =7.6 Hz, 2 H, ArH), 7.35 (t, J =8.0 Hz, 2 H, ArH), 7.83 (d, J = 8.6 Hz, 2 H, ArH). ^{13}C NMR (100 MHz, CDCl$_3$, TMS standard): δ (ppm) 11.28, 14.10, 23.08, 24.23, 29.19, 30.85, 39.58, 70.39, 105.08, 114.01, 125.06, 126.87, 154.88. HRMS(FAB) Calcd for C$_{26}$H$_{40}$O$_2$ [M$^+$]: m/z 384.3028, Found: m/z 384.3034. Elemental analysis; calculated for C$_{26}$H$_{40}$O$_2$: C 81.20, H 10.48, Found: C 81.18, H 10.80.
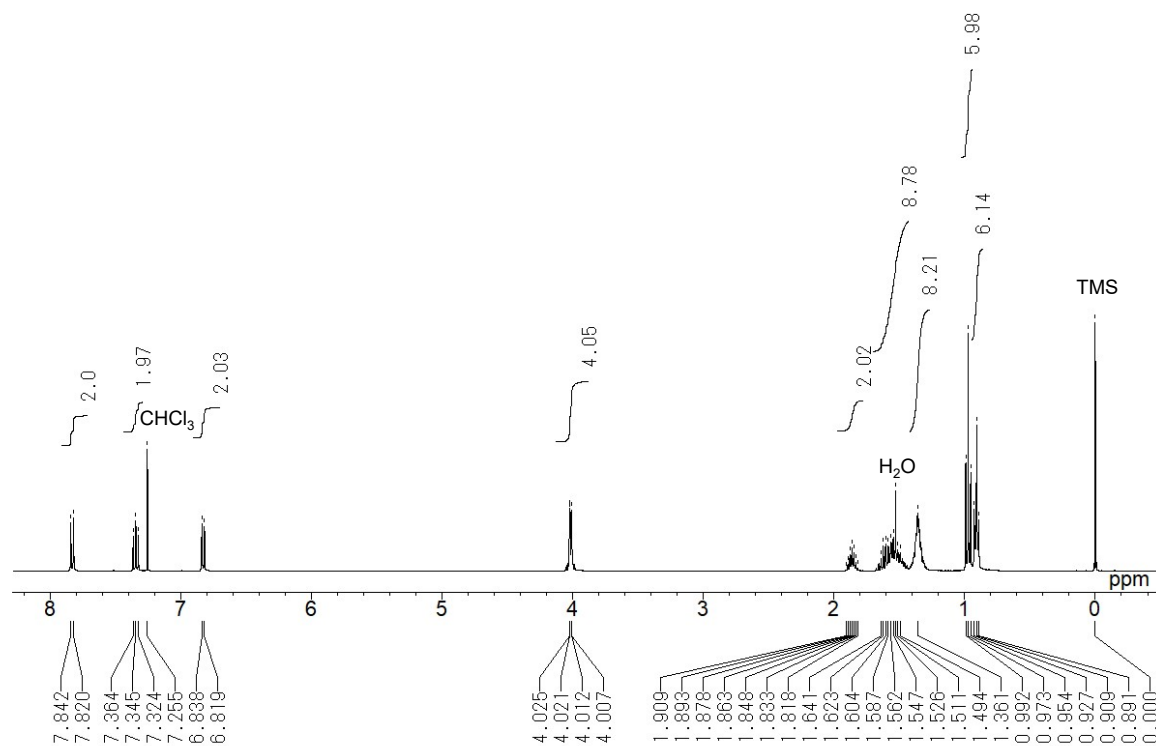
^{1}H NMR spectrum (400 MHz, CDCl$_3$, TMS standard) of **DAN**.
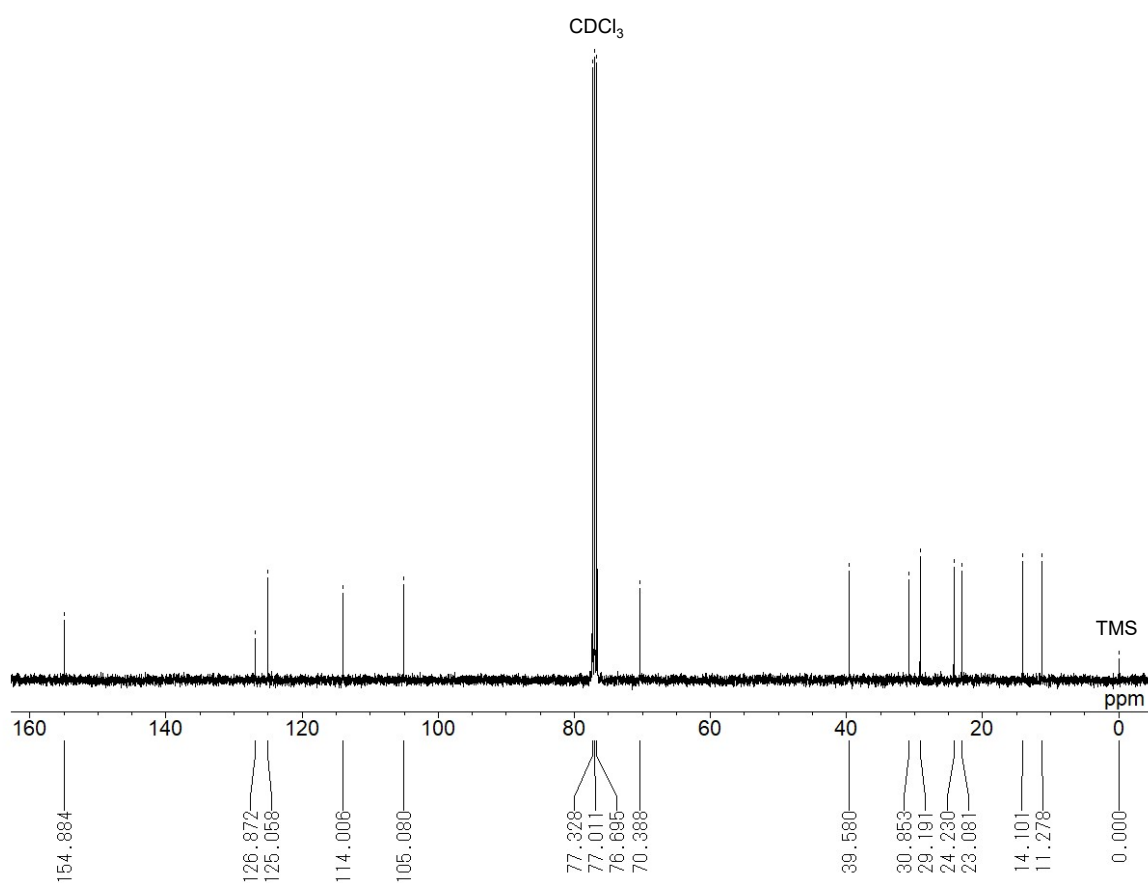
^{13}C NMR spectrum (100 MHz, CDCl$_3$, TMS standard) of **DAN**.
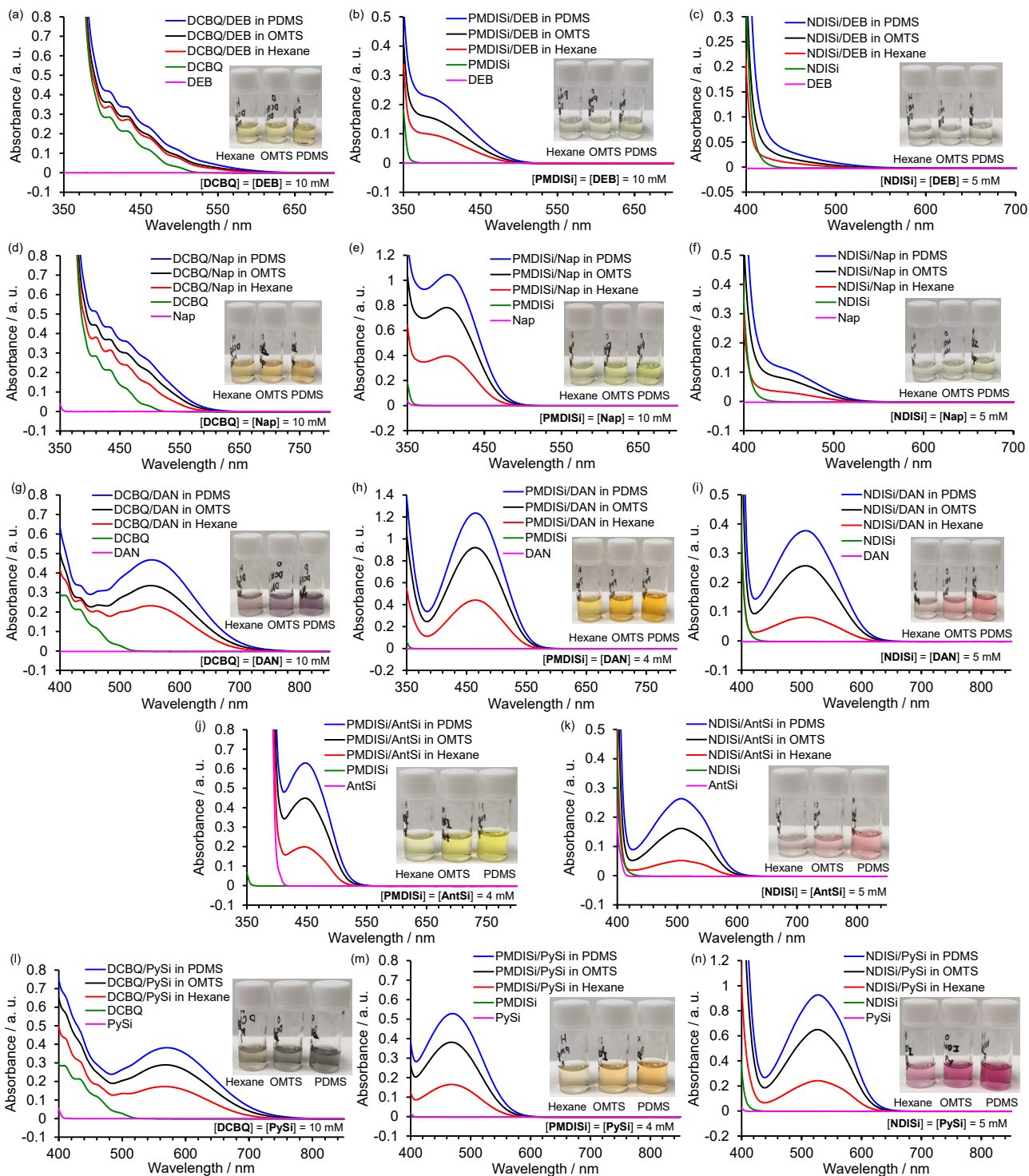
Fig. S1. Absorption spectra of acceptor in OMTS (green), donor in OMTS (magenta) and the mixture of donor and acceptor in PDMS (blue), in OMTS (black) or in *n*-hexane (red) as the solvents in system of (a) **DCBQ-DEB**, (b) **PMDISi-DEB**, (c) **NDISi-DEB**, (d) **DCBQ-Nap**, (e) **PMDISi-Nap**, (f) **NDISi-Nap**, (g) **DCBQ-DAN**, (h) **PMDISi-DAN**, (i) **NDISi-DAN**, (j) **PMDISi-AntSi**, (k) **NDISi-AntSi**, (l) **DCBQ-PySi**, (m) **PMDISi-PySi** and (n) **NDISi-PySi** at 25 °C. Photographs showing the appearance of the solutions containing the donor and acceptor in PDMS (right), OMTS (center) and *n*-hexane (left).
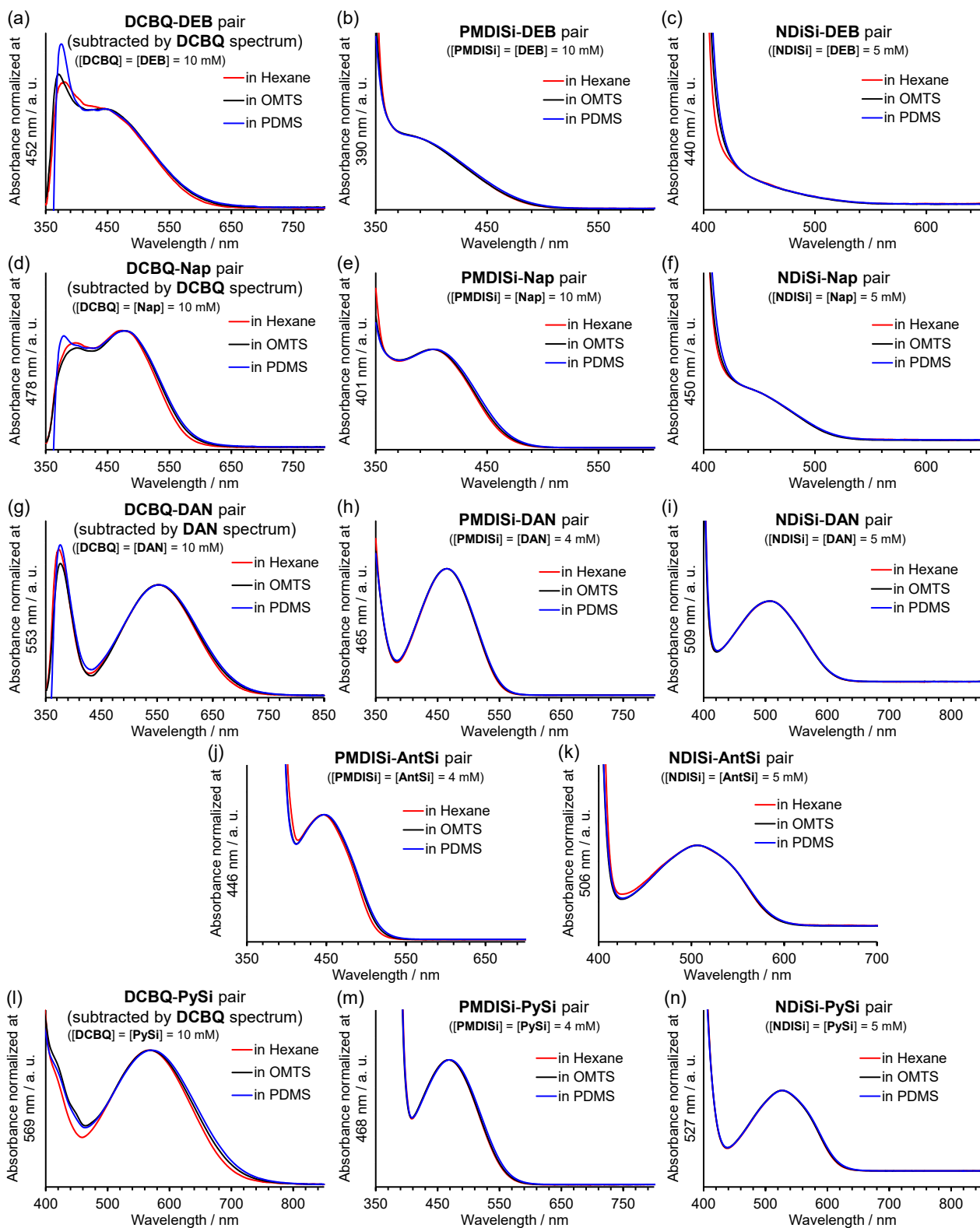
Fig. S2. Normalized absorption spectra of mixture of donor and acceptor in *n*-hexane (red), OMTS (black) and PDMS (blue) in system of (a) **DCBQ-DEB**, (b) **PMDISi-DEB**, (c) **NDiSi-DEB**, (d) **DCBQ-Nap**, (e) **PMDISi-Nap**, (f) **NDiSi-Nap**, (g) **DCBQ-DAN**, (h) **PMDISi-DAN**, (i) **NDiSi-DAN**, (j) **PMDISi-AntSi**, (k) **NDiSi-AntSi**, (l) **DCBQ-PySi**, (m) **PMDISi-PySi** and (n) **NDiSi-PySi**. The absorption spectra of **DCBQ-DEB**, **DCBQ-Nap**, **DCBQ-DAN**, **DCBQ-PySi** pairs were subtracted by spectra of **DCBQ** solutions. 25 °C.

Evaluation of the association constant

The association constant (K_a) for the CT complexes were determined by measuring the absorbance of charge transfer absorption at different concentration of the solute. All measurements were carried out at 25 °C using cuvette with 1 cm path length. The association constants were evaluated by using non-linear curve fitting of the absorbance based on the equation S1 derived from a 1:1 binding model.

$$Absorbance = \frac{\varepsilon_{CT}l\left\{[A]_0 + [D]_0 + \dfrac{1}{K_a} - \sqrt{([A]_0 + [D]_0 + \dfrac{1}{K_a})^2 - 4[A]_0[D]_0}\right\}}{2} \quad (eq.\,S1)$$

where $[D]_0$, $[A]_0$, ε_{CT} and l are initial concentration of donor and acceptor molecules, molar absorption coefficient of the CT complexes and optical path length respectively. To avoid an influence of 1:2 complex, the fittings were performed at low concentration of the donors at which saturation fractions were less than 0.55.

The sample for evaluation of the association constant were prepared by a dilution of initial solution containing the acceptor and the donor with the acceptor solution, in which the initial concentration of donor was large excess against the concentration of acceptor. And the initial concentration of donor was properly selected depending on the association constants of the solvent systems. All measurements were carried out after standing the samples more than 5 min at 25 °C. The CT absorption of CT complexes with DCBQ were overlapped with the absorption of DCBQ, the absorbance for the calculation using eq. S1 was subtracted by the absorbance of DCBQ. The calculated value of ε_{CT} of the CT complexes with DCBQ indicated difference between ε of the CT complexes and DCBQ.
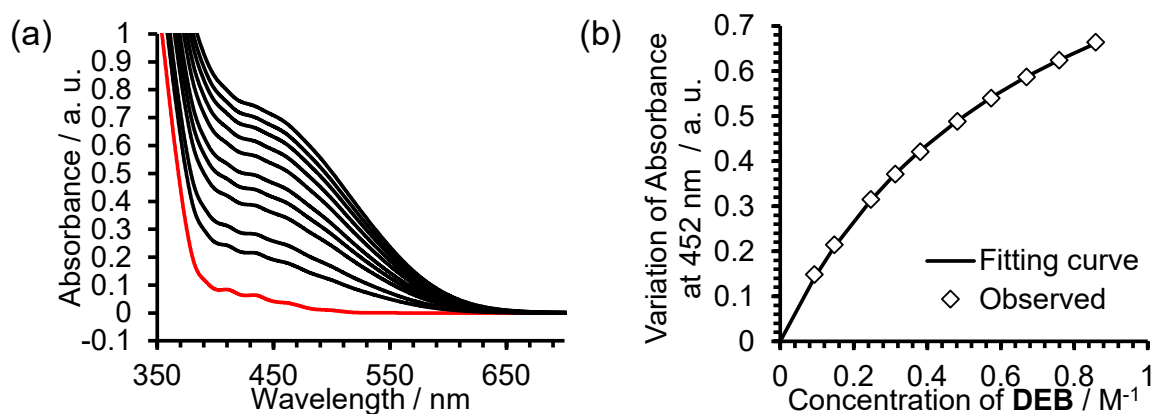
Fig. S3. (a) Absorption spectra of **DCBQ-DEB** system (black) depending on concentration of **DEB** and absorption spectrum of **DCBQ** (red) in *n*-hexane. (b) Non-linear curve fitting of the variation of absorbance of charge-transfer absorption.
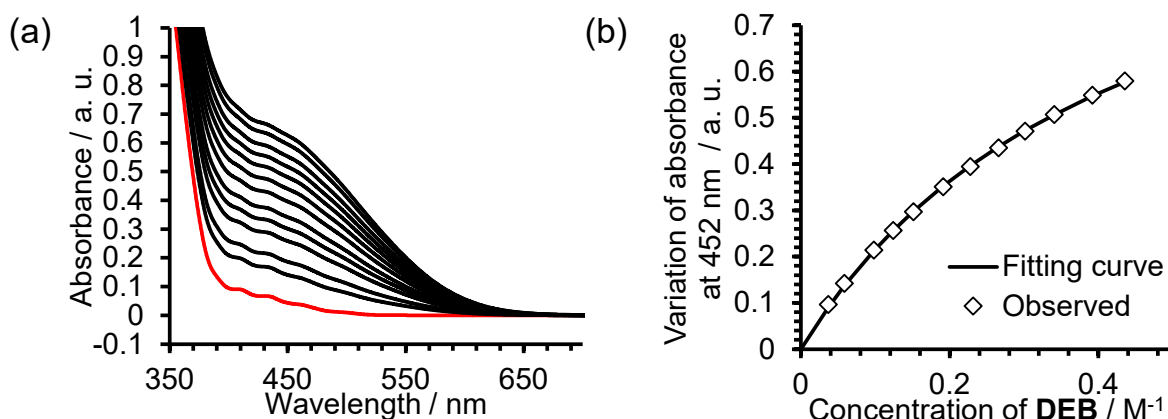
Fig. S4. (a) Absorption spectra of **DCBQ-DEB** system (black) depending on concentration of **DEB** and absorption spectrum of **DCBQ** (red) in OMTS. (b) Non-linear curve fitting of the variation of absorbance of charge-transfer absorption.
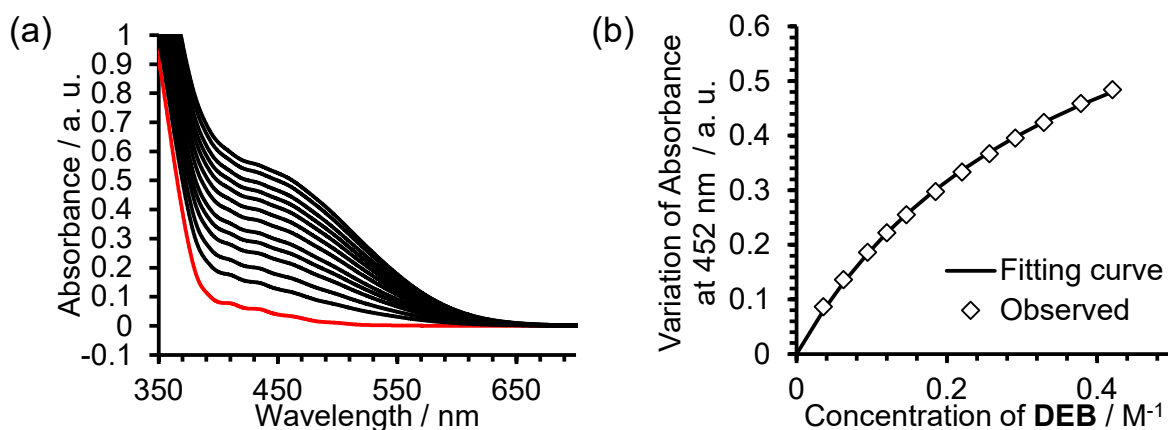
Fig. S5. (a) Absorption spectra of **DCBQ-DEB** system (black) depending on concentration of **DEB** and absorption spectrum of **DCBQ** (red) in PDMS. (b) Non-linear curve fitting of the variation of absorbance of charge-transfer absorption.
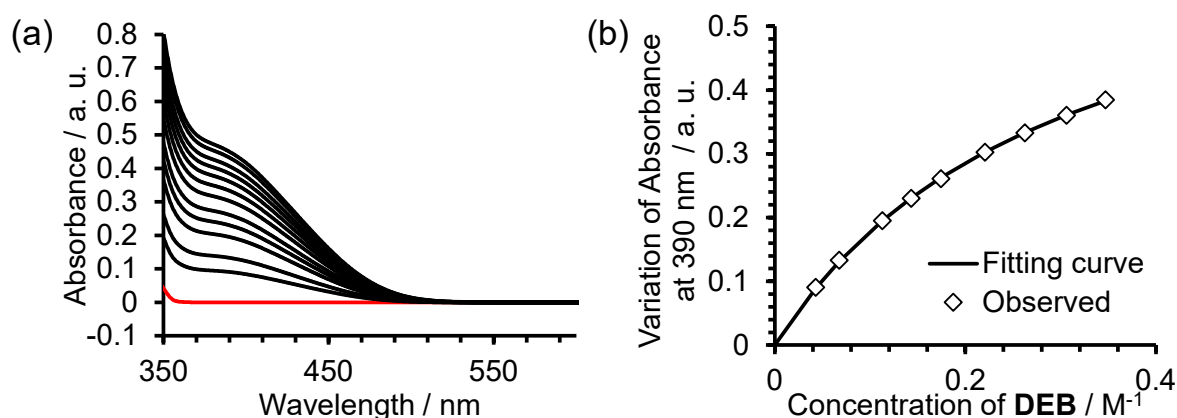
Fig. S6. (a) Absorption spectra of **PMDISi-DEB** system (black) depending on concentration of **DEB** and absorption spectrum of **PMDISi** (red) in *n*-hexane. (b) Non-linear curve fitting of the variation of absorbance of charge-transfer absorption.
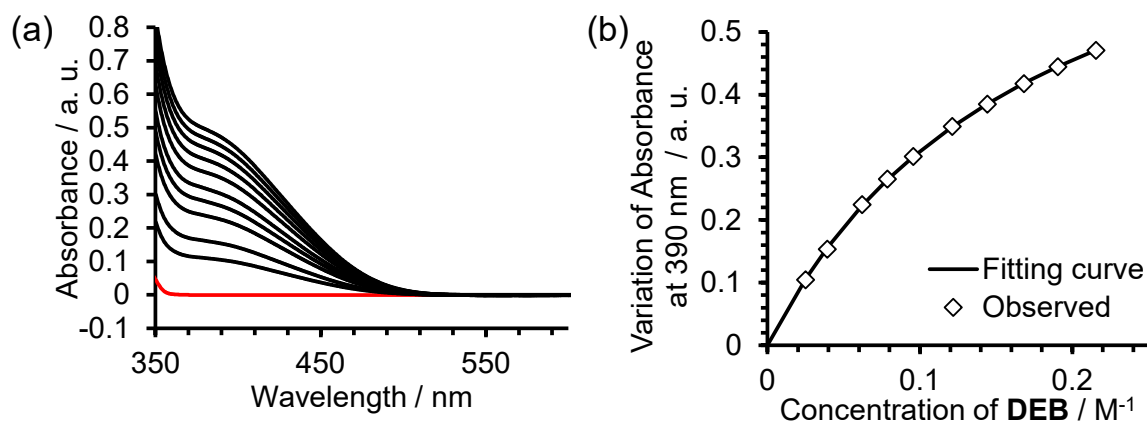
Fig. S7. (a) Absorption spectra of **PMDISi-DEB** system (black) depending on concentration of **DEB** and absorption spectrum of **PMDISi** (red) in OMTS. (b) Non-linear curve fitting of the variation of absorbance of charge-transfer absorption.
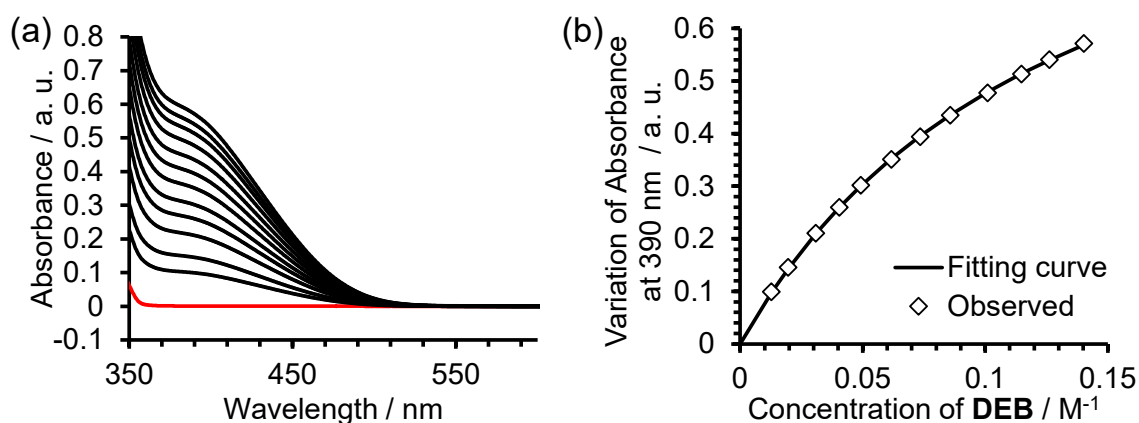
Fig. S8. (a) Absorption spectra of **PMDISi-DEB** system (black) depending on concentration of **DEB** and absorption spectrum of **PMDISi** (red) in PDMS. (b) Non-linear curve fitting of the variation of absorbance of charge-transfer absorption.
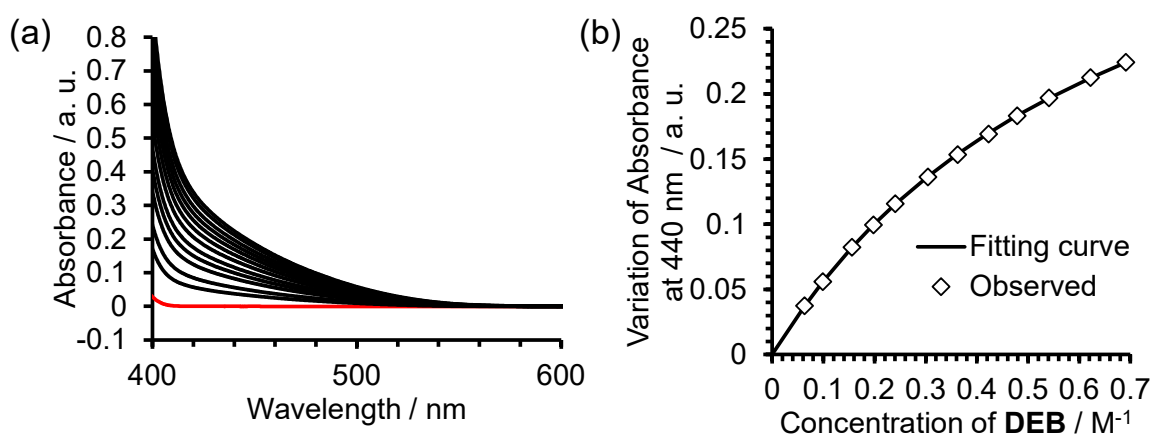
Fig. S9. (a) Absorption spectra of **NDISi-DEB** system (black) depending on concentration of **DEB** and absorption spectrum of **NDISi** (red) in *n*-hexane. (b) Non-linear curve fitting of the variation of absorbance of charge-transfer absorption.
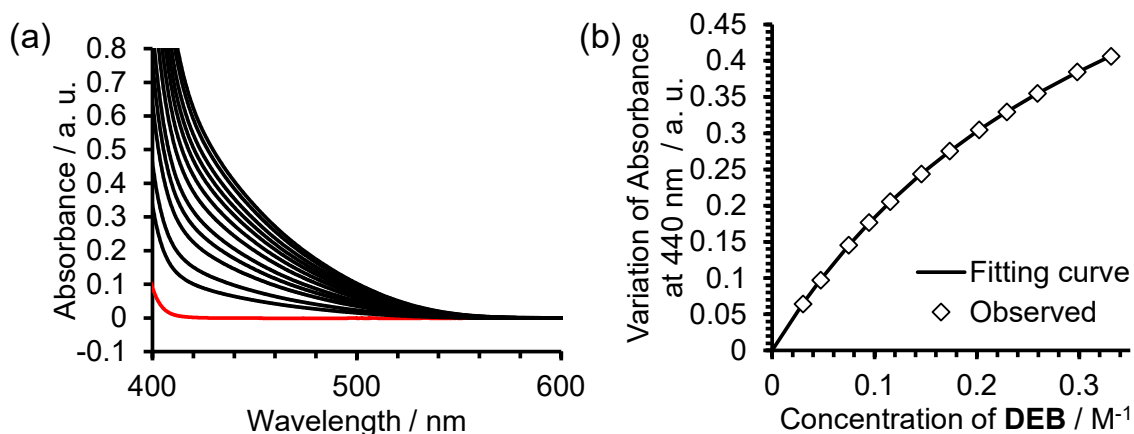
Fig. S10. (a) Absorption spectra of **NDISi-DEB** system (black) depending on concentration of **DEB** and absorption spectrum of **NDISi** (red) in OMTS. (b) Non-linear curve fitting of the variation of absorbance of charge-transfer absorption.
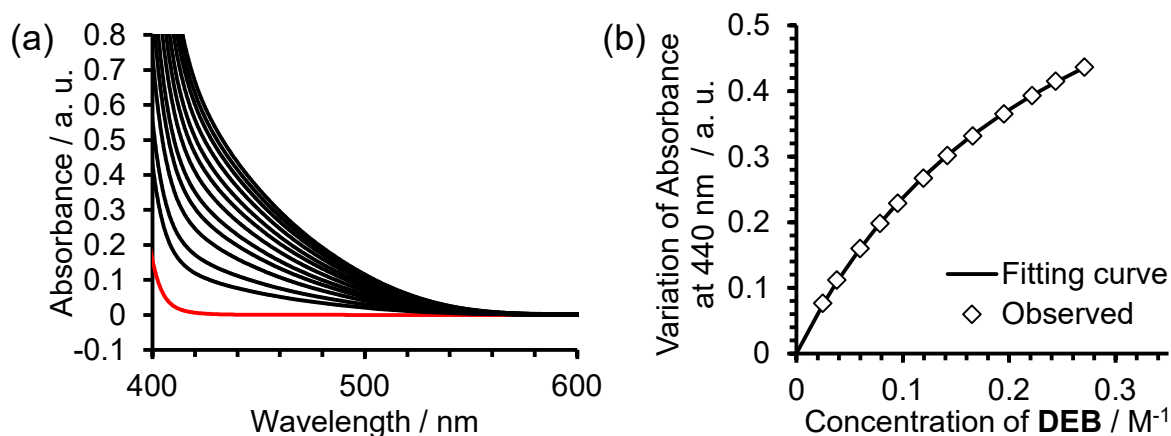
Fig. S11. (a) Absorption spectra of **NDISi-DEB** system (black) depending on concentration of **DEB** and absorption spectrum of **NDISi** (red) in PDMS. (b) Non-linear curve fitting of the variation of absorbance of charge-transfer absorption.
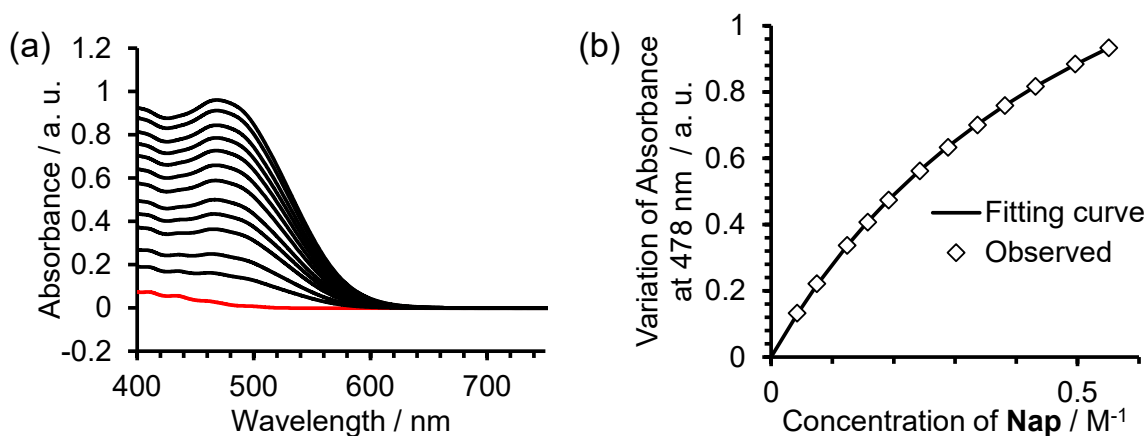
Fig. S12. (a) Absorption spectra of **DCBQ-Nap** system (black) depending on concentration of **Nap** and absorption spectrum of **DCBQ** (red) in *n*-hexane. (b) Non-linear curve fitting of the variation of absorbance of charge-transfer absorption.
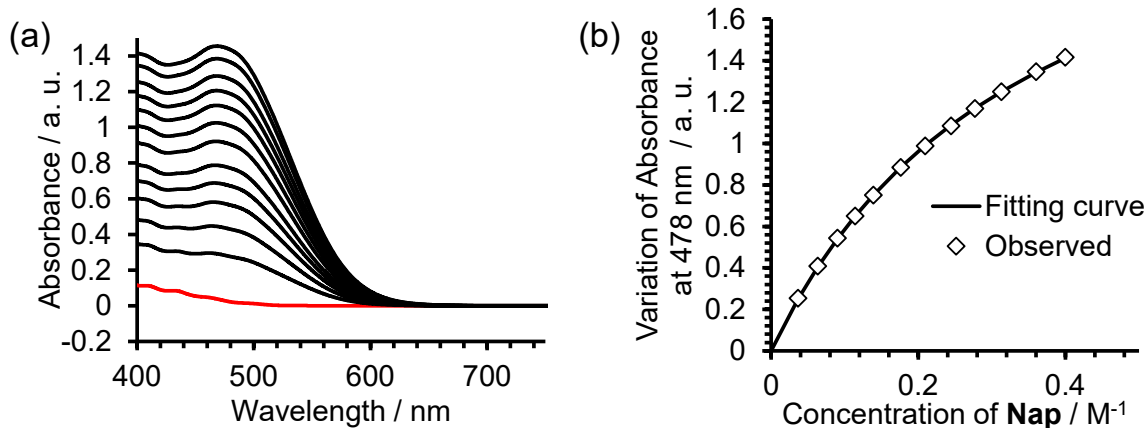
Fig. S13. (a) Absorption spectra of **DCBQ**-**Nap** system (black) depending on concentration of **Nap** and absorption spectrum of **DCBQ** (red) in OMTS. (b) Non-linear curve fitting of the variation of absorbance of charge-transfer absorption.
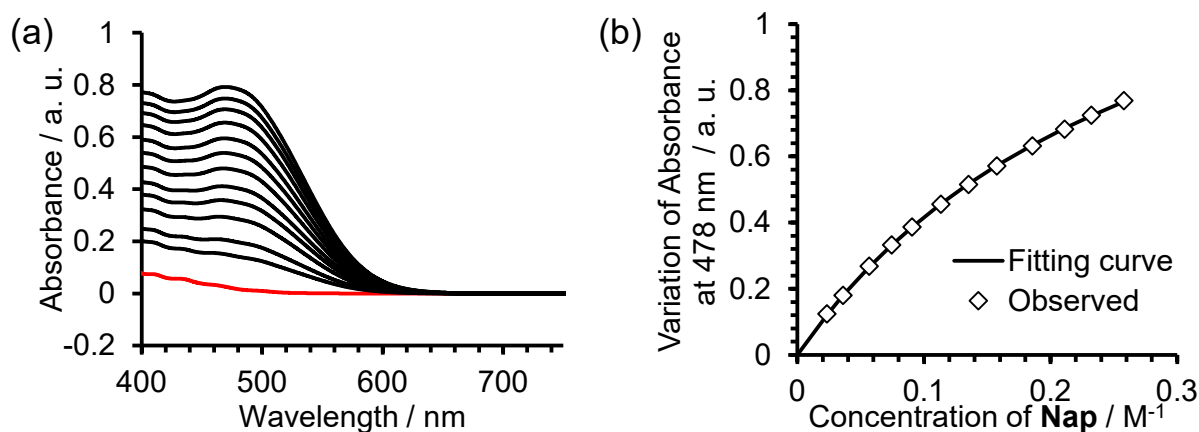
Fig. S14. (a) Absorption spectra of **DCBQ**-**Nap** system (black) depending on concentration of **Nap** and absorption spectrum of **DCBQ** (red) in PDMS. (b) Non-linear curve fitting of the variation of absorbance of charge-transfer absorption.
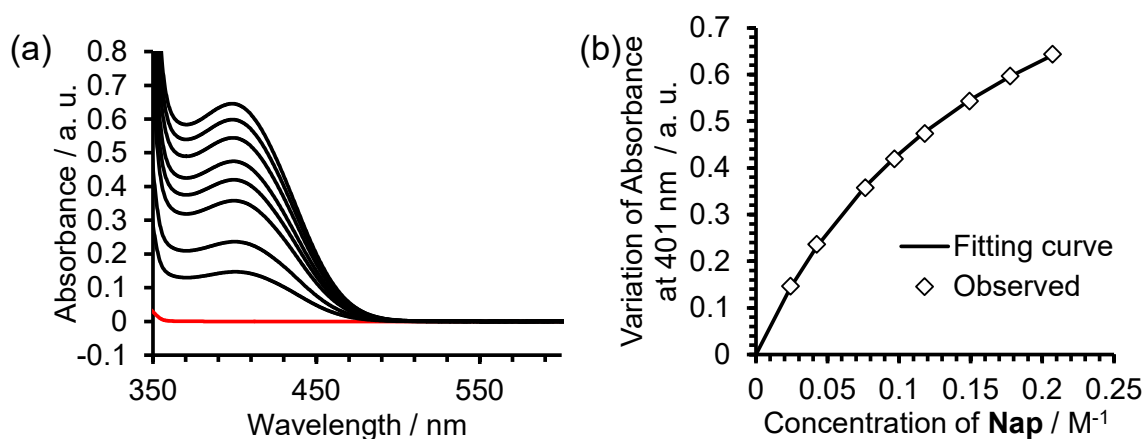
Fig. S15. (a) Absorption spectra of **PMDISi**-**Nap** system (black) depending on concentration of **Nap** and absorption spectrum of **PMDISi** (red) in *n*-hexane. (b) Non-linear curve fitting of the variation of absorbance of charge-transfer absorption.
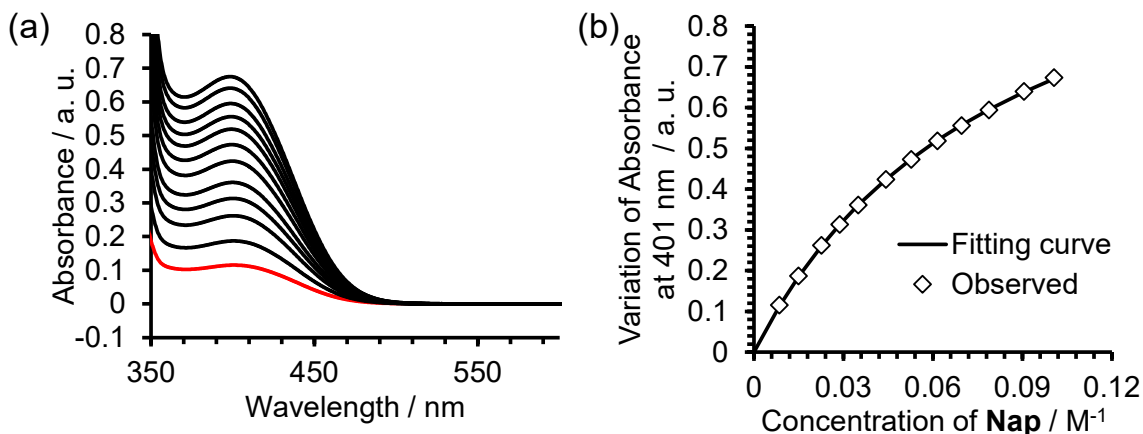
Fig. S16. (a) Absorption spectra of **PMDISi**-**Nap** system (black) depending on concentration of **Nap** and absorption spectrum of **PMDISi** (red) in OMTS. (b) Non-linear curve fitting of the variation of absorbance of charge-transfer absorption.
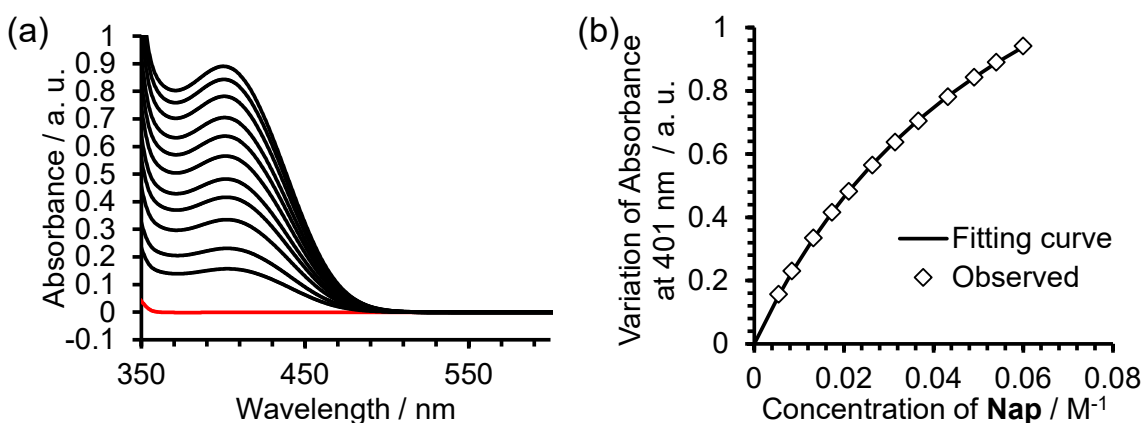
Fig. S17. (a) Absorption spectra of **PMDISi**-**Nap** system (black) depending on concentration of **Nap** and absorption spectrum of **PMDISi** (red) in PDMS. (b) Non-linear curve fitting of the variation of absorbance of charge-transfer absorption.
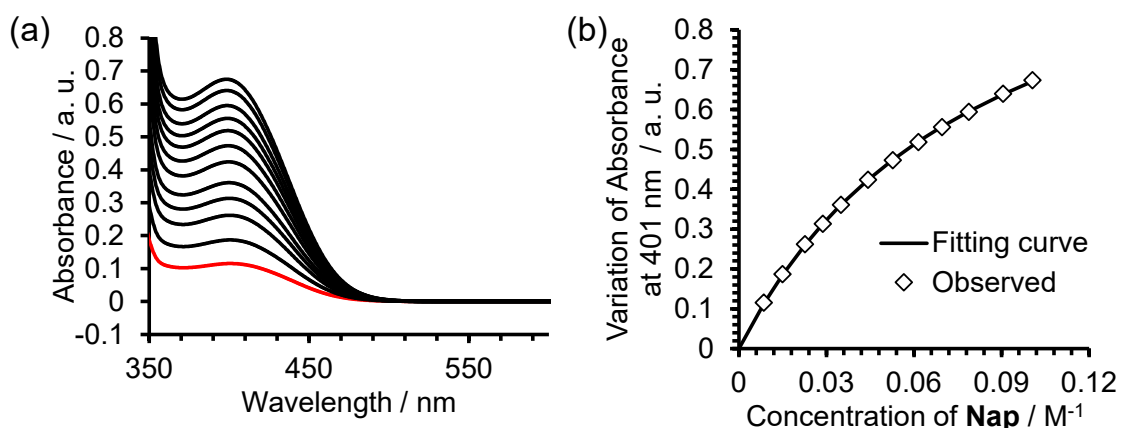
Fig. S18. (a) Absorption spectra of **NDISi**-**Nap** system (black) depending on concentration of **Nap** and absorption spectrum of **NDISi** (red) in *n*-hexane. (b) Non-linear curve fitting of the variation of absorbance of charge-transfer absorption.
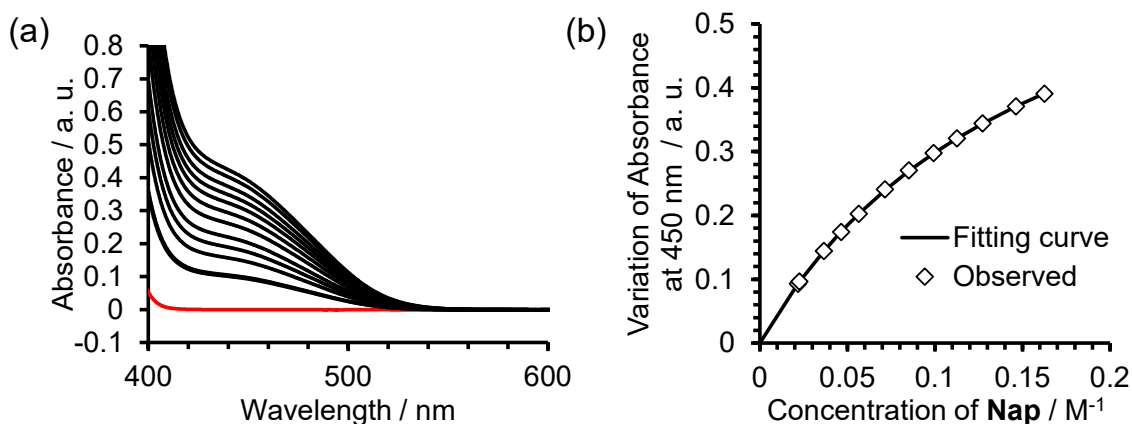
Fig. S19. (a) Absorption spectra of **NDISi-Nap** system (black) depending on concentration of **Nap** and absorption spectrum of **NDISi** (red) in OMTS. (b) Non-linear curve fitting of the variation of absorbance of charge-transfer absorption.
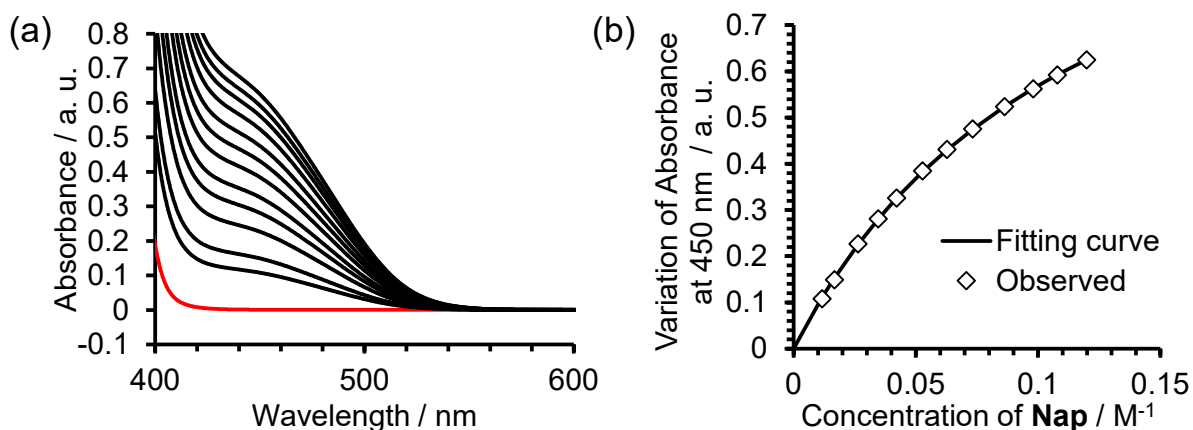
Fig. S20. (a) Absorption spectra of **NDISi-Nap** system (black) depending on concentration of **Nap** and absorption spectrum of **NDISi** (red) in PDMS. (b) Non-linear curve fitting of the variation of absorbance of charge-transfer absorption.
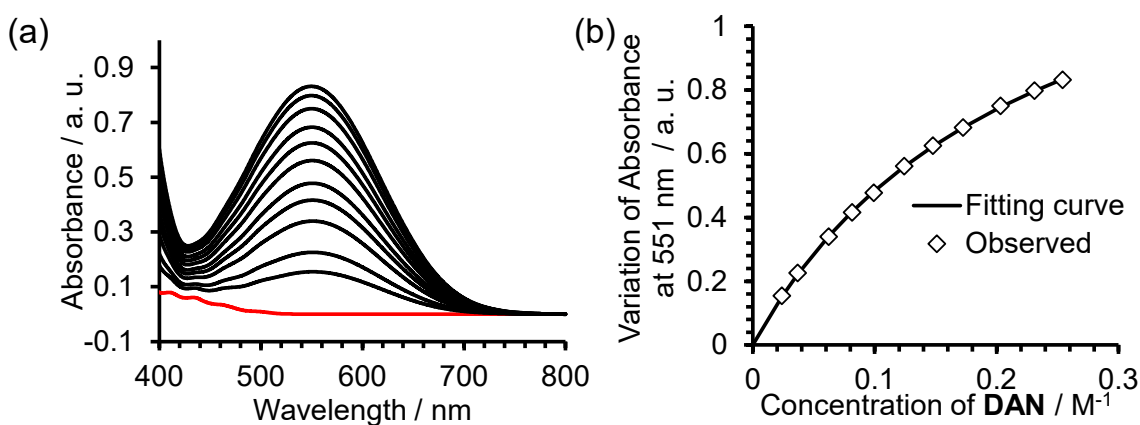
Fig. S21. (a) Absorption spectra of **DCBQ-DAN** system (black) depending on concentration of **DAN** and absorption spectrum of **DCBQ** (red) in *n*-hexane. (b) Non-linear curve fitting of the variation of absorbance of charge-transfer absorption.
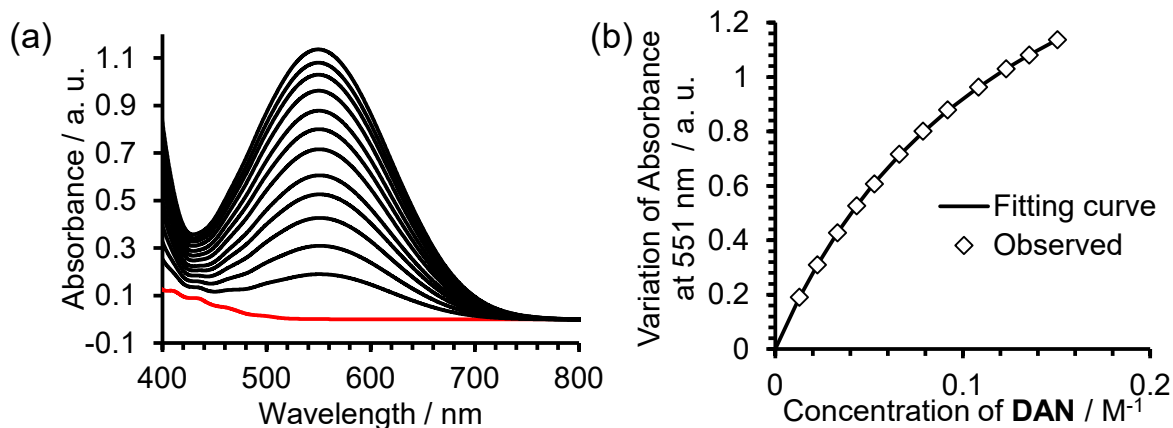
Fig. S22. (a) Absorption spectra of **DCBQ-DAN** system (black) depending on concentration of **DAN** and absorption spectrum of **DCBQ** (red) in OMTS. (b) Non-linear curve fitting of the variation of absorbance of charge-transfer absorption.
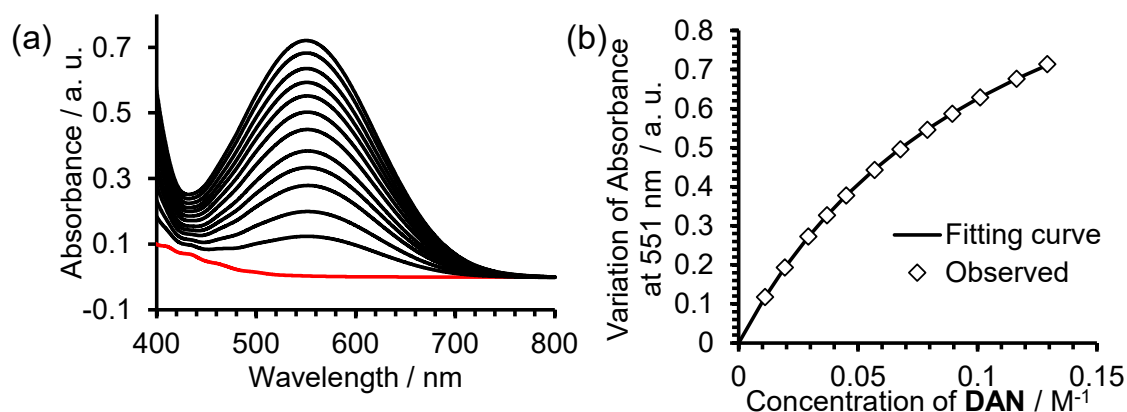
Fig. S23. (a) Absorption spectra of **DCBQ-DAN** system (black) depending on concentration of **DAN** and absorption spectrum of **DCBQ** (red) in PDMS. (b) Non-linear curve fitting of the variation of absorbance of charge-transfer absorption.
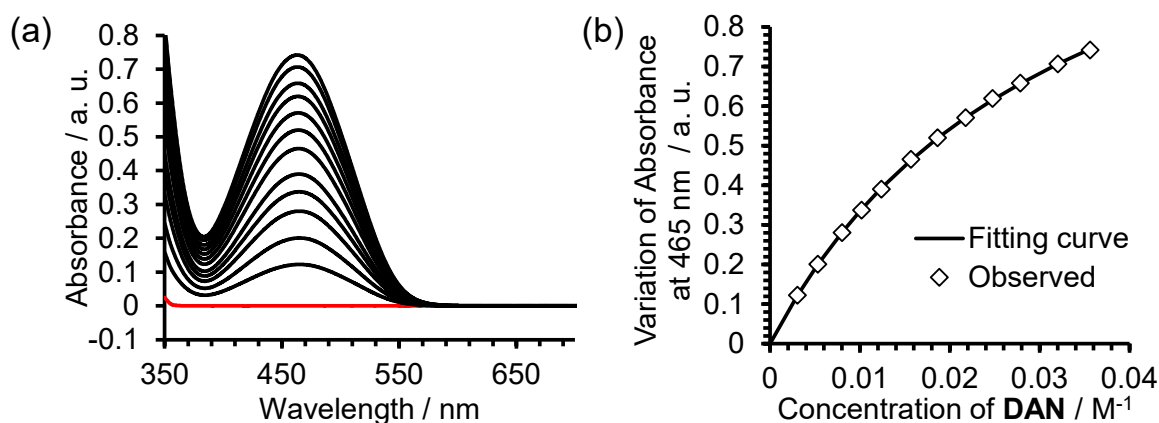
Fig. S24. (a) Absorption spectra of **PMDISi-DAN** system (black) depending on concentration of **DAN** and absorption spectrum of **PMDISi** (red) in *n*-hexane. (b) Non-linear curve fitting of the variation of absorbance of charge-transfer absorption.
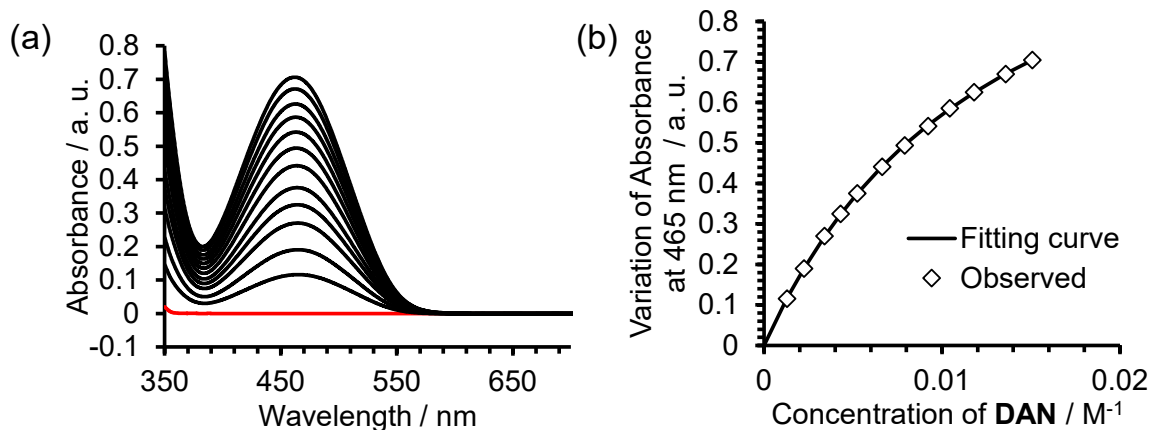
Fig. S25. (a) Absorption spectra of **PMDISi-DAN** system (black) depending on concentration of **DAN** and absorption spectrum of **PMDISi** (red) in OMTS. (b) Non-linear curve fitting of the variation of absorbance of charge-transfer absorption.
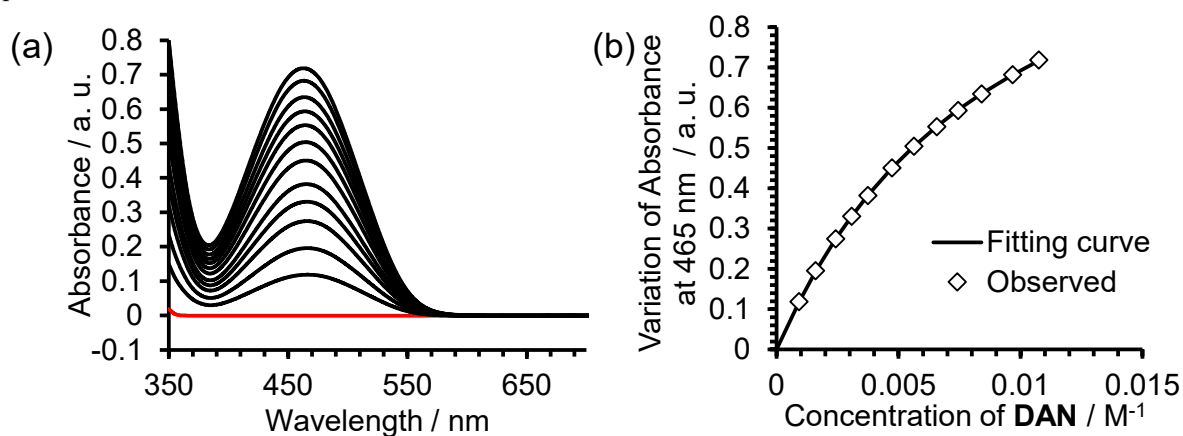
Fig. S26. (a) Absorption spectra of **PMDISi-DAN** system (black) depending on concentration of **DAN** and absorption spectrum of **PMDISi** (red) in PDMS. (b) Non-linear curve fitting of the variation of absorbance of charge-transfer absorption.
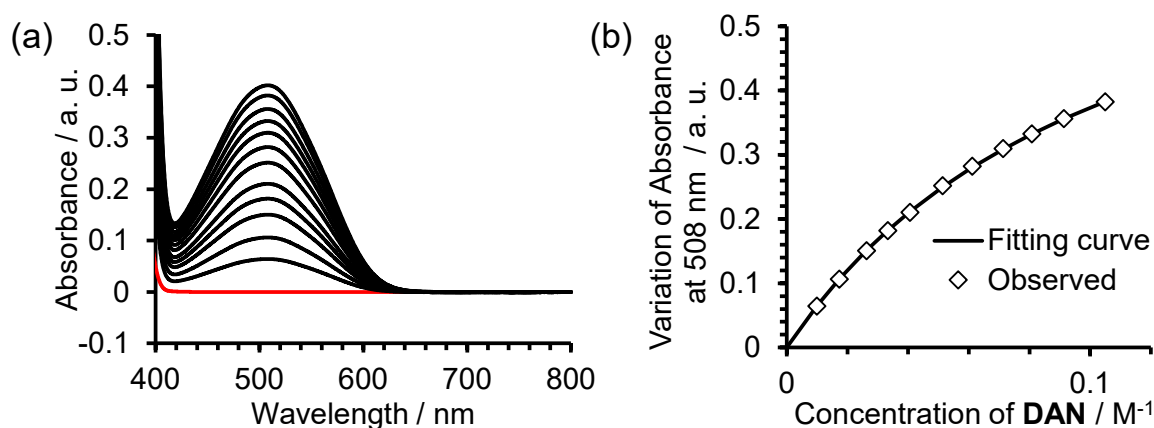
Fig. S27. (a) Absorption spectra of **NDISi-DAN** system (black) depending on concentration of **DAN** and absorption spectrum of **NDISi** (red) in *n*-hexane. (b) Non-linear curve fitting of the variation of absorbance of charge-transfer absorption.
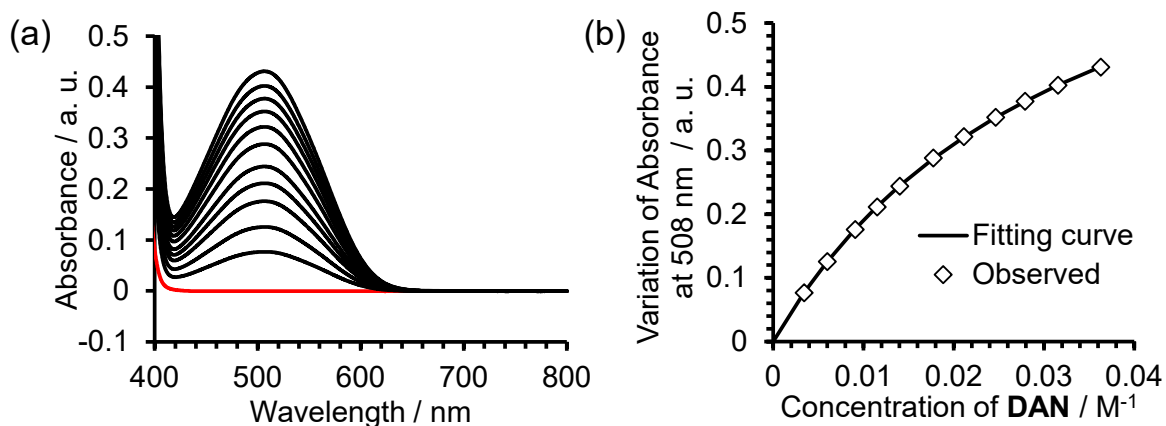
Fig. S28. (a) Absorption spectra of **NDISi-DAN** system (black) depending on concentration of **DAN** and absorption spectrum of **NDISi** (red) in OMTS. (b) Non-linear curve fitting of the variation of absorbance of charge-transfer absorption.
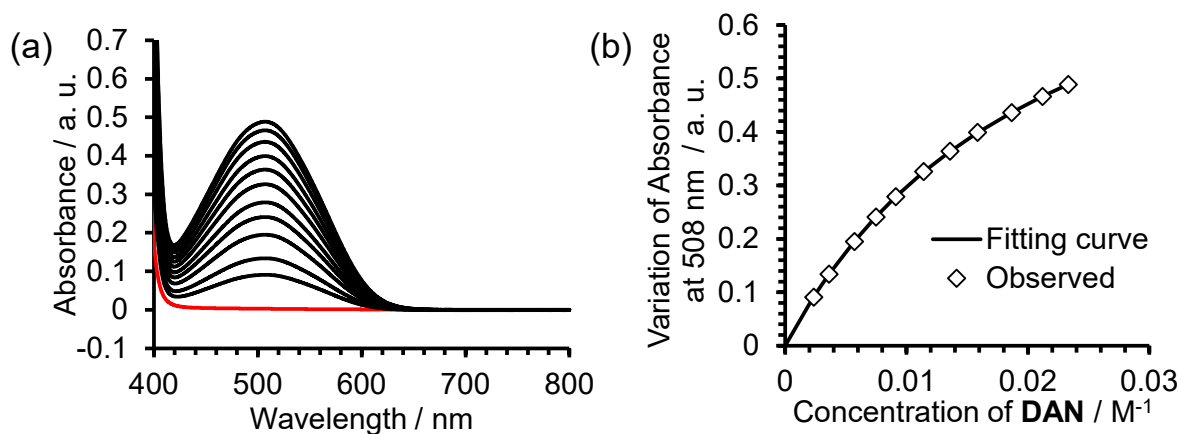
Fig. S29. (a) Absorption spectra of **NDISi-DAN** system (black) depending on concentration of **DAN** and absorption spectrum of **NDISi** (red) in PDMS. (b) Non-linear curve fitting of the variation of absorbance of charge-transfer absorption.
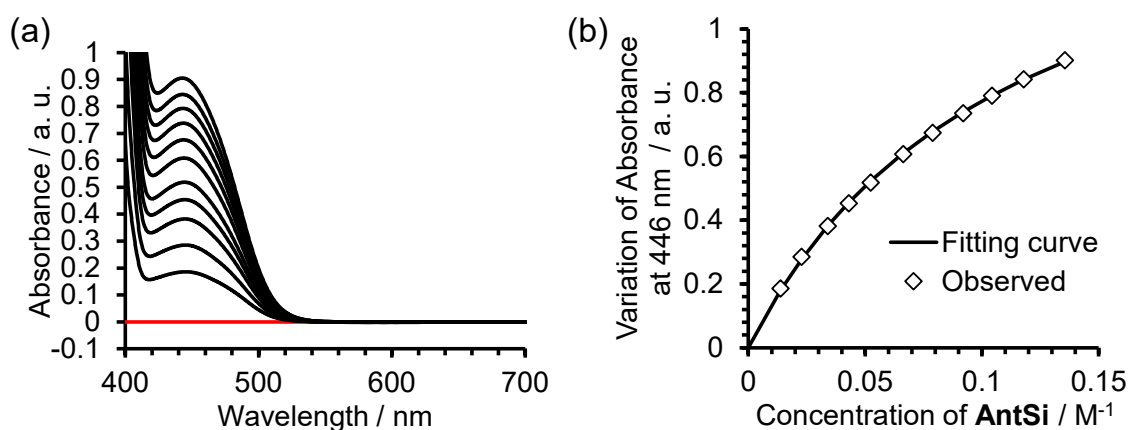
Fig. S30. (a) Absorption spectra of **PMDISi-AntSi** system (black) depending on concentration of **AntSi** and absorption spectrum of **PMDISi** (red) in *n*-hexane. (b) Non-linear curve fitting of the variation of absorbance of charge-transfer absorption.
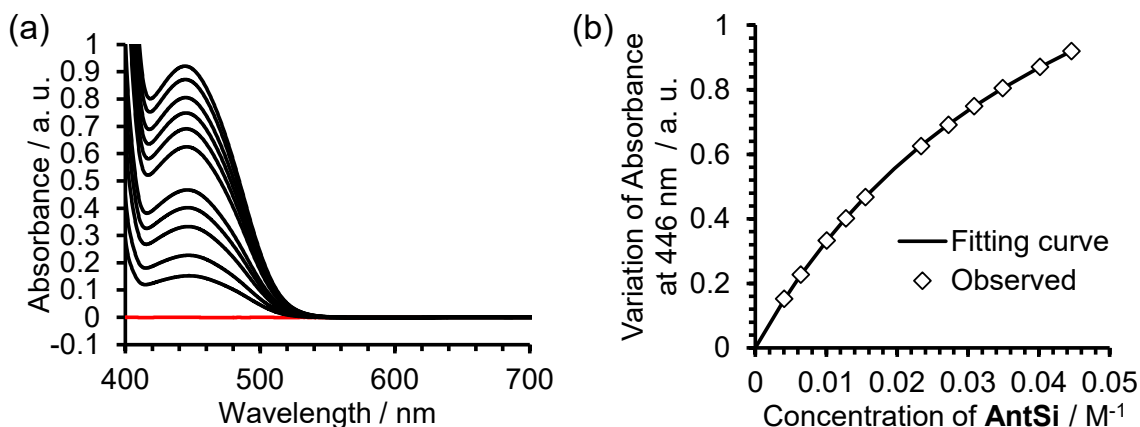
Fig. S31. (a) Absorption spectra of **PMDISi**-**AntSi** system (black) depending on concentration of **AntSi** and absorption spectrum of **PMDISi** (red) in OMTS. (b) Non-linear curve fitting of the variation of absorbance of charge-transfer absorption.
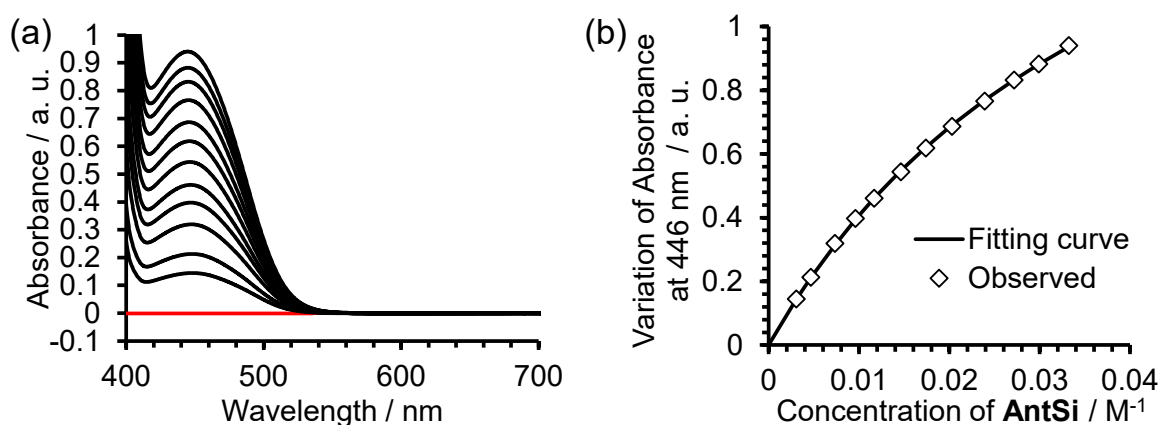
Fig. S32. (a) Absorption spectra of **PMDISi**-**AntSi** system (black) depending on concentration of **AntSi** and absorption spectrum of **PMDISi** (red) in PDMS. (b) Non-linear curve fitting of the variation of absorbance of charge-transfer absorption.
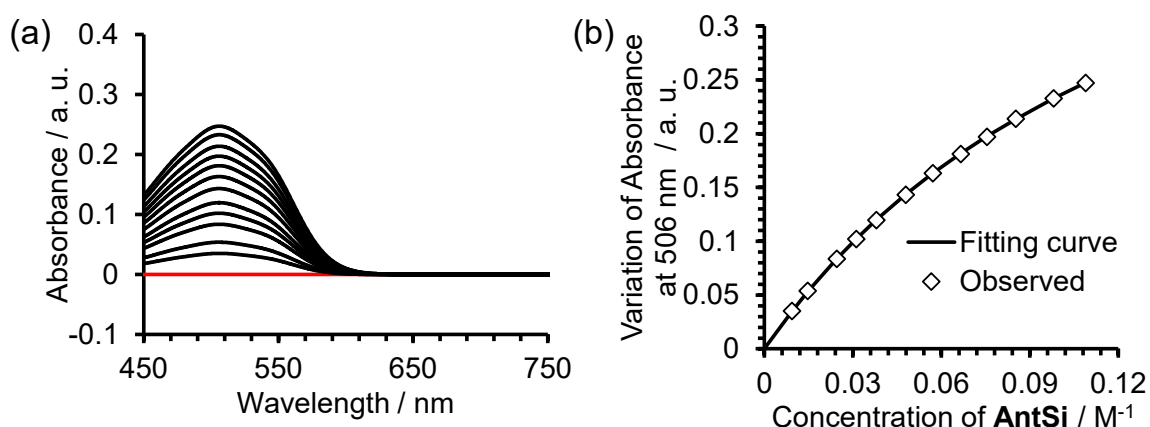
Fig. S33. (a) Absorption spectra of **NDISi**-**AntSi** system (black) depending on concentration of **AntSi** and absorption spectrum of **NDISi** (red) in *n*-hexane. (b) Non-linear curve fitting of the variation of absorbance of charge-transfer absorption.
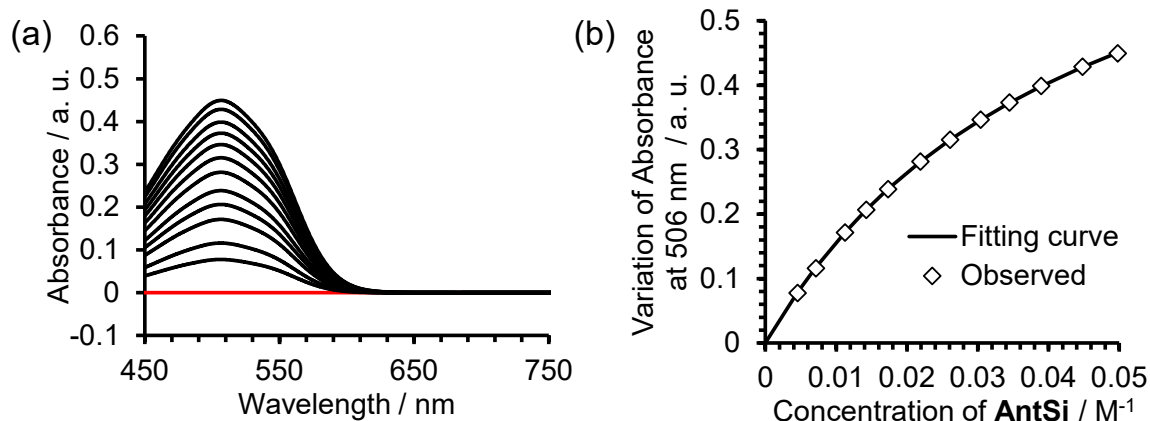
Fig. S34. (a) Absorption spectra of **NDISi**-**AntSi** system (black) depending on concentration of **AntSi** and absorption spectrum of **NDISi** (red) in OMTS. (b) Non-linear curve fitting of the variation of absorbance of charge-transfer absorption.
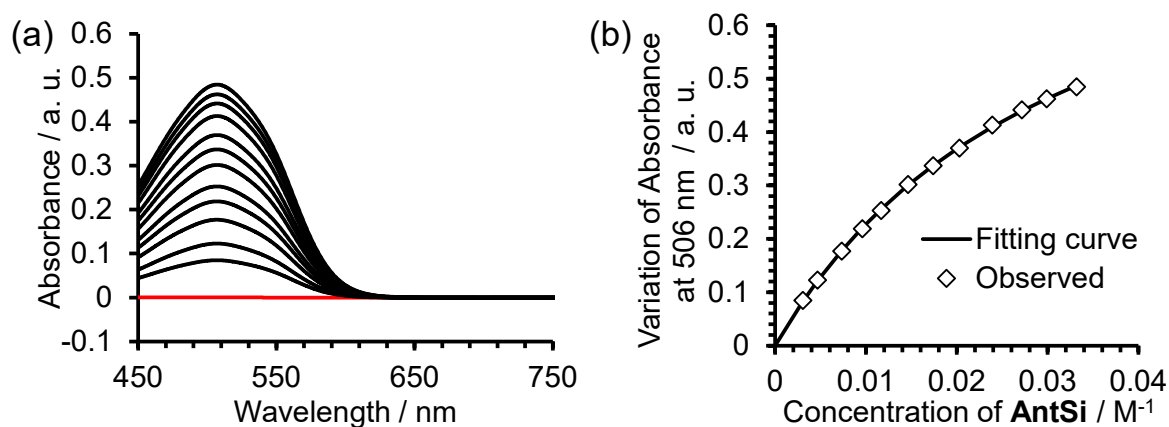
Fig. S35. (a) Absorption spectra of **NDISi**-**AntSi** system (black) depending on concentration of **AntSi** and absorption spectrum of **NDISi** (red) in PDMS. (b) Non-linear curve fitting of the variation of absorbance of charge-transfer absorption.
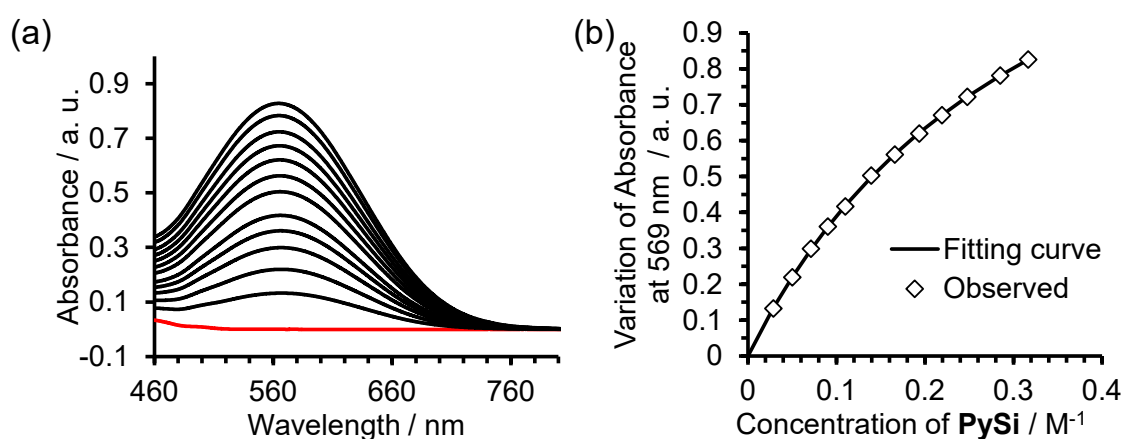
Fig. S36. (a) Absorption spectra of **DCBQ**-**PySi** system (black) depending on concentration of **PySi** and absorption spectrum of **DCBQ** (red) in *n*-hexane. (b) Non-linear curve fitting of the variation of absorbance of charge-transfer absorption.
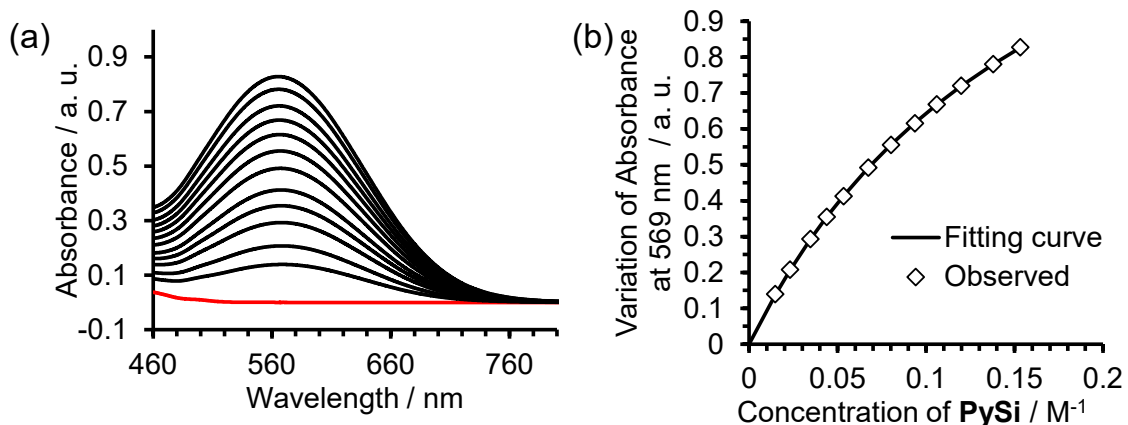
Fig. S37. (a) Absorption spectra of **DCBQ**-**PySi** system (black) depending on concentration of **PySi** and absorption spectrum of **DCBQ** (red) in OMTS. (b) Non-linear curve fitting of the variation of absorbance of charge-transfer absorption.
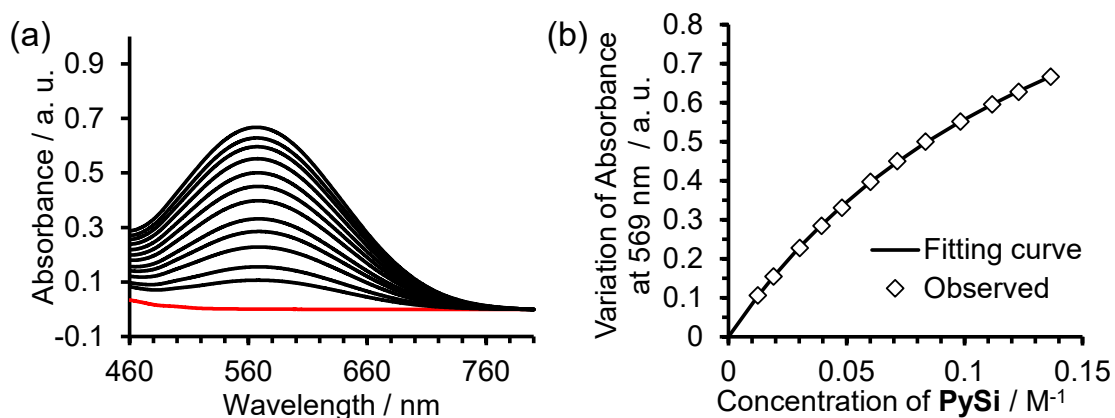
Fig. S38. (a) Absorption spectra of **DCBQ**-**PySi** system (black) depending on concentration of **PySi** and absorption spectrum of **DCBQ** (red) in PDMS. (b) Non-linear curve fitting of the variation of absorbance of charge-transfer absorption.
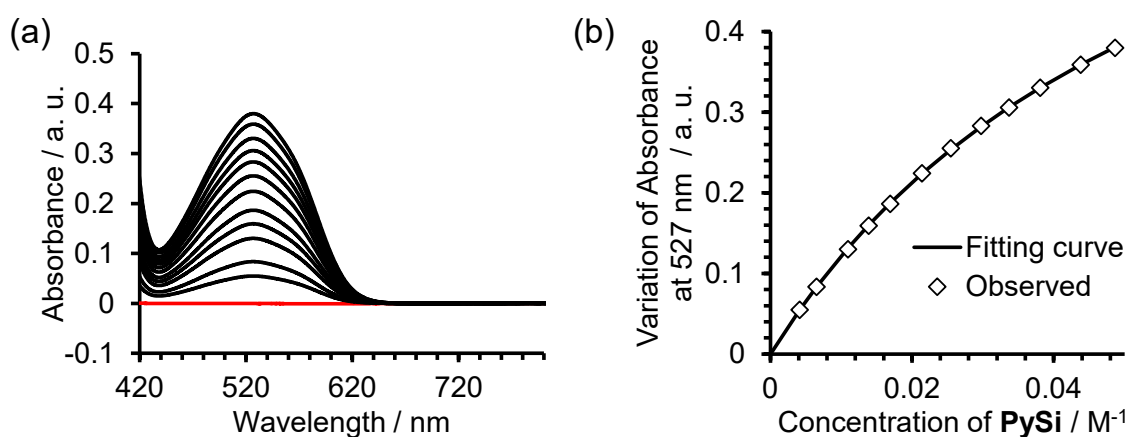
Fig. S39. (a) Absorption spectra of **NDISi**-**PySi** system (black) depending on concentration of **PySi** and absorption spectrum of **NDISi** (red) in *n*-hexane. (b) Non-linear curve fitting of the variation of absorbance of charge-transfer absorption.
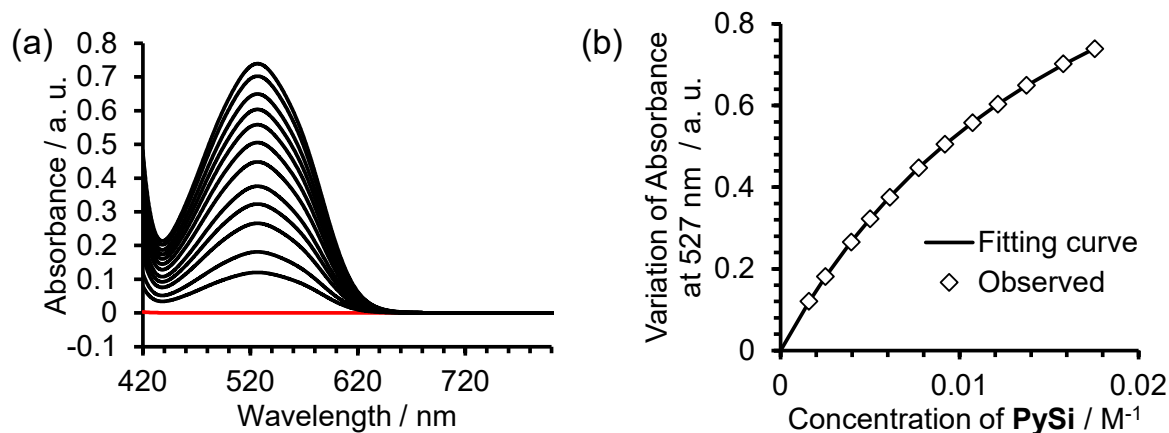
Fig. S40. (a) Absorption spectra of **NDISi-PySi** system (black) depending on concentration of **PySi** and absorption spectrum of **NDISi** (red) in OMTS. (b) Non-linear curve fitting of the variation of absorbance of charge-transfer absorption.
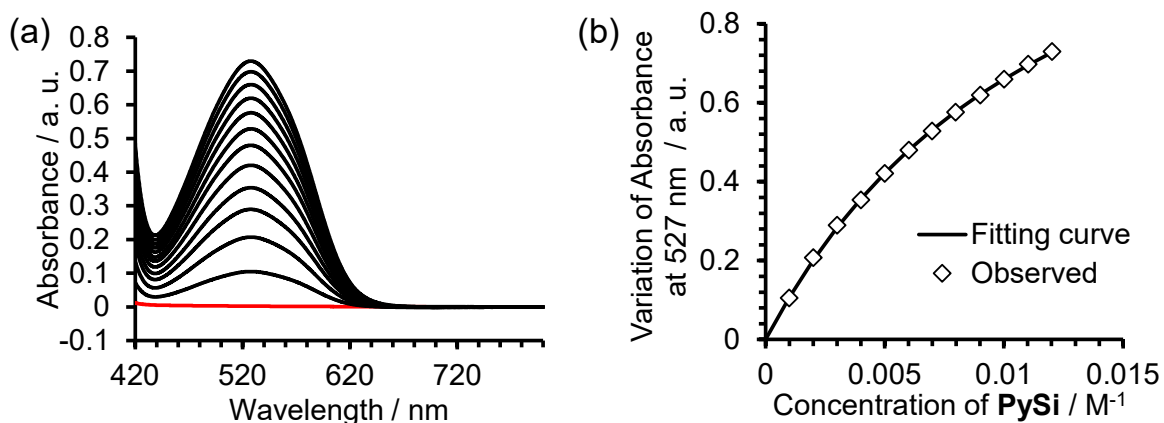
Fig. S41. (a) Absorption spectra of **NDISi-PySi** system (black) depending on concentration of **PySi** and absorption spectrum of **NDISi** (red) in PDMS. (b) Non-linear curve fitting of the variation of absorbance of charge-transfer absorption.

Table S1. Molar absorption coefficient of the CT complexes calculated by using eq. S1.

DA pair	ε_{CT} (M^{-1} cm^{-1})[a]			DA pair	ε_{CT} (M^{-1} cm^{-1})[a]		
	n-hexane	OMTS	PDMS		*n*-hexane	OMTS	PDMS
DCBQ-DEB	400[b] (450 nm)	370[b] (450 nm)	390[b] (450 nm)	**PMDISi-AntSi**	1500 (445 nm)	1600 (445 nm)	1700 (445 nm)
DCBQ-Nap	690[b] (475 nm)	700[b] (475 nm)	700[b] (475 nm)	**PMDISi-PySi**	520 (468 nm)	480 (468 nm)	480 (468 nm)
DCBQ-DAN	560[b] (551 nm)	540[b] (551 nm)	570[b] (551 nm)	**NDISi-DEB**	400 (440 nm)	410 (440 nm)	400 (440 nm)
DCBQ-PySi	600[b] (567 nm)	570[b] (567 nm)	630[b] (567 nm)	**NDISi-Nap**	520 (450 nm)	530 (450 nm)	580 (450 nm)
PMDISi-DEB	310 (390 nm)	320 (390 nm)	320 (390 nm)	**NDISi-DAN**	410 (508 nm)	430 (508 nm)	460 (508 nm)
PMDISi-Nap	770 (401 nm)	790 (401 nm)	830 (401 nm)	**NDISi-AntSi**	390 (506 nm)	390 (506 nm)	430 (506 nm)
PMDISi-DAN	1100 (465 nm)	1100 (465 nm)	1200 (465 nm)	**NDISi-PySi**	690 (527 nm)	670 (527 nm)	700 (527 nm)

[a] Wavelength of CT absorption for non-linear curve fitting in parentheses. [b] The values of ε_{CT} of the CT complexes with DCBQ indicated difference between ε_{CT} of the CT complexes and DCBQ due to overlap between the CT absorption and the absorption of DCBQ.

	PMDISi	NDISi	DCBQ					
Number of atoms of aromatic core	16	20	8					
	DEB	Nap	DAN	AntSi	PySi			
Number of atoms of aromatic core	6	10	10	14	16			
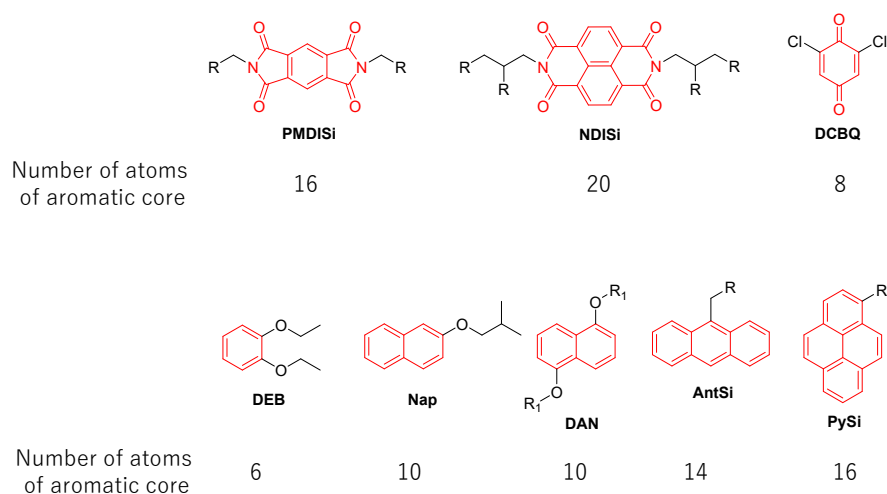
Fig. S42. Number of atoms of aromatic core using the CT complexes. The selected atoms of the core were indicated in red.

Reference

1. S. Amemori, K. Kikuchi and M. Mizuno, *Chem. Commun.*, 2021, **57**, 1141.
2. S. Loser, H. Miyauchi, J. W. Hennek, J. Smith, C. Huang, A. Facchetti and T. J. Marks, *Chem. Commun.*, 2012, **48**, 8511.